An Allosteric Shift in CD11c Affinity Activates a Proatherogenic State in Arrested Intermediate Monocytes

Alfredo A. Hernandez,* Greg A. Foster,* Stephanie R. Soderberg,* Andrea Fernandez,* Mack B. Reynolds,* Mable K. Orser,* Keith A. Bailey,* Jason H. Rogers,† Gagan D. Singh,† Huaizhu Wu,‡ Anthony G. Passerini,* and Scott I. Simon*

Intermediate monocytes (iMo; $CD14^+CD16^+$) increase in number in the circulation of patients with unstable coronary artery disease (CAD), and their recruitment to inflamed arteries is implicated in events leading to mortality following MI. Monocyte recruitment to inflamed coronary arteries is initiated by high affinity β2-integrin (CD11c/CD18) that activates β1-integrin (VLA-4) to bind endothelial VCAM-1. How integrin binding under shear stress mechanosignals a functional shift in iMo toward an inflammatory phenotype associated with CAD progression is unknown. Whole blood samples from patients treated for symptomatic CAD including non-ST elevation MI, along with healthy age-matched subjects, were collected to assess chemokine and integrin receptor levels on monocytes. Recruitment on inflamed human aortic endothelium or rVCAM-1 under fluid shear stress was assessed using a microfluidic-based artery on a chip (A-Chip). Membrane upregulation of high affinity CD11c correlated with concomitant activation of VLA-4 within focal adhesive contacts was required for arrest and diapedesis across inflamed arterial endothelium to a greater extent in non-ST elevation MI compared with stable CAD patients. The subsequent conversion of CD11c from a high to low affinity state under fluid shear activated phospho-Syk– and ADAM17-mediated proteolytic cleavage of CD16. This marked the conversion of iMo to an inflammatory phenotype associated with nuclear translocation of NF-κB and production of $IL\text{-}1\beta^+$. We conclude that CD11c functions as a mechanoregulator that activates an inflammatory state preferentially in a majority of iMo from cardiac patients but not healthy patients. ***The Journal of Immunology*****, 2020, 205: 2806–2820.**

The pathogenesis of atherosclerosis is largely a function of the interplay of persistent activation of the vascular endothelium and recruitment of monocytes within hydrodynamically susceptible arterial regions where low shear stress or unsteady blood flow persist (1). Monocyte recruitment to these regions is initiated by uptake of atherogenic lipoproteins and signaling of integrin receptor function via ligation of chemokine receptors (i.e., CCR2) (2, 3). Adhesive and signaling functions of these integrins can then drive monocyte transmigration and subsequent polarization and differentiation that are critical for the progression of coronary artery disease (CAD) (4, 5).

Of the integrins involved in leukocyte arrest to arterial endothelium under shear stress, β_2-integrin CD11c/CD18 and β_1-integrin CD29/CD49d (VLA-4) both recognize VCAM-1 upregulated on hydrodynamically susceptible coronary arteries (6). Shear-resistant arrest is mediated by a cooperative process between CD11c and VLA-4 that involves Syk phosphorylation and downstream binding of paxillin to the α_4 cytoplasmic tail, which supports bond formation to VCAM-1 at focal adhesions (7). Mice susceptible to hyperlipidemia upregulate CD11c on circulating monocytes that participate in the development of nascent plaques (8, 9). Additionally, these same ApoE and LDL null mice deficient in the CD11c gene exhibit diminished arterial inflammation characterized by fewer foamy macrophages and significantly less plaque burden.

Of the monocyte subsets that circulate in humans, intermediate monocytes (iMo; $CD14^{hi}$, $CD16^{hi}$, $CCR2^{hi}$, and $HLA\text{-}DR^{int}$) are the most efficient at upregulating membrane CD11c following internalization of lipoproteins or stimulation with chemokine. An increase in the number of circulating iMo correlate with a higher frequency of cardiovascular complications, including reinfarction and heart failure (10–14). In the circulation, CD11c upregulated on iMo in response to the uptake of TGRL or ligation of chemokine receptor shifts from a low affinity to a high affinity conformation that promotes VLA-4–dependent adhesion to VCAM-1 (12). Moreover, CD11c expression increases in direct proportion to the efficiency of iMo arrest and measures of cardiovascular injury in coronary patients with

*Department of Biomedical Engineering, University of California, Davis, Davis, CA 95616; †Department of Cardiovascular and Internal Medicine, University of California, Davis Medical Center, Sacramento, CA 95817; and ‡Section of Cardiovascular Research, Department of Medicine, Baylor College of Medicine, Houston, TX 77030

ORCIDs: 0000-0002-8445-3749 (M.B.R.); 0000-0002-7833-7012 (M.K.O.); 0000-0003-3363-8070 (J.H.R.); 0000-0001-6846-5531 (H.W.); 0000-0001-8007-4672 (A.G.P.); 0000-0003-1186-6611 (S.I.S.).

Received for publication April 29, 2020. Accepted for publication September 10, 2020.

This work was supported by National Institutes of Health, National Institute of Allergy and Infectious Diseases Grant AI047294 (to S.I.S.) and National Heart, Lung, and Blood Institute Grants HL082689 (to A.G.P. and S.I.S.) and HL098839 (to H.W.).

A.A.H., G.A.F., and S.I.S. designed the study and led the study and wrote the manuscript. G.D.S., J.H.R., S.I.S., A.F., M.B.R., M.K.O., S.R.S., and K.A.B. assisted in patient identification and recruitment as well as the acquisition of blood samples. S.I.S., A.G.P., and H.W. provided critical input on study design and provided key edits to the manuscript, which was approved by all authors.

Address correspondence and reprint requests to Prof. Scott I. Simon, Department of Biomedical Engineering, University of California, Davis, 451 E. Health Sciences Drive, Davis, CA 95616. E-mail address: sisimon@ucdavis.edu

The online version of this article contains supplemental material.

Abbreviations used in this article: AF, Alexa Fluor; CAD, coronary artery disease; CK-MB, serum creatine kinase; cMo, classical monocyte; HAEC, human aortic endothelial cell; iMo, intermediate monocyte; LAD, left anterior descending; LVEF%, left ventricular ejection fraction; MFI, mean fluorescence intensity; MI, myocardial infarction; ncMo, nonclassical monocyte; NSTEMI, non–ST segment; PCA, principal component analysis; TEM, transendothelial migration; TIRF, total internal reflection fluorescence.

established disease (i.e., necrotic core volume, creatine kinase, and troponin) (2, 3, 15).

We have previously reported that high affinity CD11c mechanotransduces the activation of kinase (i.e., phospho-Syk), resulting in the recruitment of cytoskeletal adaptor proteins paxillin and the consolidation of VLA-4 bound to VCAM-1 to support shear-resistant monocyte arrest and the subsequent transendothelial migration (TEM) (15). Previous reports have also documented that outside-in signaling via β_1-integrins including VLA-4 on monocytes can activate the NF-κB signaling pathway (16–19). This in turn initiates the transcription of inflammatory genes (e.g., *c-fos* and *c-jun)* that promote expression of components of the NLRP3 inflammasome and pro–IL-1β, resulting in cellular conversion to an inflammatory phenotype (18, 20). The mechanism underlying how integrins and other receptors that concentrate within lipid rafts at sites of focal adhesion participate in the conversion of arrested monocytes into inflammatory macrophages capable of producing TNF-α, IL-1β, and IL-6 within nascent plaques has not been established (21, 22). We hypothesized that iMo represent a primed circulating population in cardiac patients and that progression from stable CAD to myocardial infarction (MI) can be gauged ex vivo by measures of β_1- and β_2-integrin activation and composition within focal adhesions that define their signaling capacity and thus regulate monocyte fate in atheroinflammation.

In the current study, we analyzed fresh whole blood samples obtained on the day of percutaneous coronary intervention in the cardiac catheterization laboratory from patients presenting with angina but otherwise stable plaque (denoted CAD) and those treated for non–ST segment MI (NSTEMI) compared with healthy age-matched subjects. Single cell analysis of integrin and chemokine receptor expression was performed via flow cytometry, and regulation of CD11c and VLA-4 adhesion function during monocyte arrest and outside-in signaling were imaged in real time using total internal reflection fluorescence (TIRF) microscopy assembled beneath artery-on-a-chip microfluidic channels (A-Chip). iMo from cardiac patients exhibited elevated expression of integrins and chemokine receptors that coincided with enhanced efficiency of recruitment and diapedesis in the A-Chip compared with healthy controls. Following arrest, an allosteric shift in CD11c from high to low affinity on arrested iMo triggered ADAM17-dependent shedding of membrane CD16 receptors that marked the conversion to a $CD14^+/CD16^-$ proatherogenic phenotype characterized by nuclear translocation of NF-κB and production of IL-1β. The capacity of iMo to arrest and convert to an inflammatory phenotype increased in patients classified as NSTEMI. Taken together, these data reveal that CD11c bonds function as mechanotransducing receptors that activate iMo toward an inflammatory state under hydrodynamic shear stress of blood flow.

Materials and Methods

Human healthy age-matched subjects

Blood samples were collected from 117 cardiac patients undergoing coronary angiography for treatment of symptomatic stable CAD (n = 56) or NSTEMI (n = 46) and healthy age-matched subjects (n = 15) between 40 and 60 y of age with no history of disease. All healthy age-matched subjects provided informed consent to participate in this Institutional Review Board–approved study at the University of California, Davis. Patients with stable CAD were diagnosed based on presentation with exertional substernal chest pressure without recent acceleration in symptoms and evidence of a significant angiographic stenosis ∼70%. Patients with MI were diagnosed by a presentation of chest pressure, electrocardiographic changes, elevated troponin consistent with NSTEMI, and angiographic evidence of a flow-limiting coronary artery stenosis. All patients with NSTEMI were treated within 12 h of the onset of initial symptoms. Synergy Between Percutaneous Coronary Intervention With Taxus and Cardiac Surgery score and lesion length were classified using quantitative coronary angiography. Myocardial blush was scored after intervention from 0 to 3. Corrected thrombolysis in myocardial infarction frame counts were also scored for each infarct-related artery.

Patient characteristics are detailed in Table I. In brief, NSTEMI patients were diagnosed with significant manifestation of disease at the level of the proximal left anterior descending (LAD) and main coronary arteries that required angioplasty and arterial stenting and a ∼2-fold longer hospital stay than CAD. NSTEMI patients were more likely to be tobacco smokers and diabetic; however, no significant difference in pharmacological intervention was noted as nearly all patients received beta blockers, angiotensin-converting enzyme inhibitors, and statins (Table I). NSTEMI patients were admitted and placed on antiplatelet and anticoagulant therapy. CAD patients treated in the cardiac clinic with complaints of chest pain were placed on antiplatelet therapy and categorized according to severity of symptoms and electrocardiogram findings. Patients experienced both right coronary artery lesions as well as LAD lesions. Patients typically received echocardiograms on the day of admission.

Blood collection

Whole blood was collected from recruited healthy age-matched subjects by venipuncture from the general population near Davis, CA. Arterial and venous whole blood from consented patients with confirmed CAD was collected at University of California, Davis Medical Center under the supervision of a practicing cardiologist on the day of catheterization into sodium heparin–coated vacutainer tubes. Blood differential counts were determined using a Coulter Act Hematology Analyzer (Beckman Coulter).

mAbs

The following Abs were purchased from BioLegend (San Diego, CA) for microscopy and flow cytometry: CD14 Alexa Fluor (AF) 488 (clone HCD14), CD16 AF700 (clone 3G8), CD11c PE conjugated/unconjugated (clone Bu15), anti-CD11c high affinity reporter (3.9) Brilliant Violet 711, CD11b PE (clone ICRF44), CD49d PerCp Cy5.5 (clone 9F10), CX3CR1 PE (clone 2A9-1), CCR2 PE (clone K036C2), CCR5 PE (clone HEK/1/85a), and IL-1β (AF647: clone H1b-98). Blocking Abs to CD11c (3.9) and VLA-4 (HP2/1) were purchased from BioLegend and GeneTex, respectively. CD11c allosteric agonist 496B, which activates CD11c, and CD11c allosteric antagonist 496K that stabilizes a low affinity space were generously provided by Elli Lilly and were used at a saturating concentration of 5 μg/ml for microfluidic studies.

Flow cytometry and principal component analysis

For classification, viable monocyte singlets were classified into their respective subsets based upon expression of HLA-DR, CCR2, CD14, and CD16 (see Fig. 1). Fifty microliters of blood was treated first with Human True Stain FcX and True Stain Monocyte Blocker (BioLegend) for 10 min, labeled with fluorescent Abs for 30 min, followed by RBC removal with lysis buffer (BioLegend). Data were acquired on an Attune NxT flow cytometer within 2 h of blood collection.

VCAM-1 coating on glass coverslips and A-Chip microfluidic device assembly

VCAM-1 coverslips served as the substrate of the A-Chip and were prepared as previously described (3). A-Chip microfluidic chambers were constructed using polydimethylsiloxane SYLGARD 184 prepolymer (Dow Corning) poured over a master mold as previously described in detail (15). Reservoir for infusion and vacuum access holes to seal the coverslip to the flow channel device were punched directly into the polydimethylsiloxane chamber using an 18-gauge needle. Following perfusion, cell arrest and TEM was gauged by phase-contrast and fluorescence microscopy. Monocyte subsets were discriminated based on the relative immunofluorescence of Abs to CD14, CD16, and CCR2 as previously reported (15).

Whole blood adhesion assay

A monocyte recruitment assay was performed using a 1:4 dilution of heparinized whole blood. Diluted blood was added to the A-Chip reservoir and perfused through the chamber by a syringe pump (Harvard Apparatus, Holliston, MA) at a flow rate resulting in a physiological shear stress of 2 dynes/cm^2 at the fluid substrate interface. Monocyte arrest was quantified based upon the mean number of cells counted per five fields at 60× magnification after 15 min of shear flow. The frequency of iMo arrest was computed from the mean count from five fields normalized by the total number infused based upon the Coulter blood count.

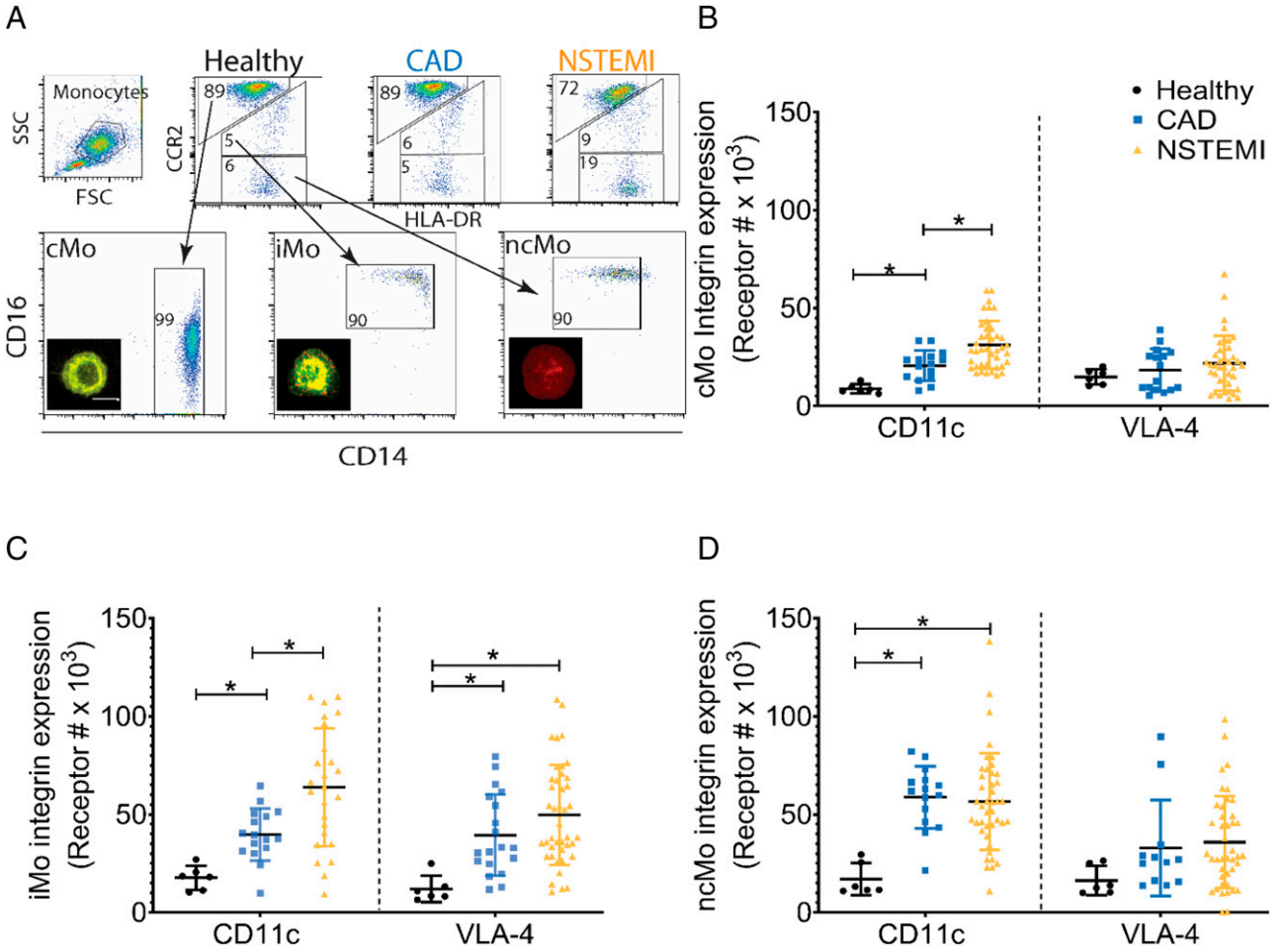

FIGURE 1. Integrin expression is elevated on monocytes from blood samples of cardiac patients compared with healthy age-matched subjects. (**A**) Gating strategy for the monocyte subsets based on expression of HLA-DR, CCR2, CD14, and CD16 applied to each patient cohort to define monocyte subsets, as indicated via representative images (CD14, green; CD16, red). Blood was collected from age-matched healthy controls ($n = 6$) and compared with CAD ($n = 16$) and NSTEMI ($n = 27$) on the day of percutaneous intervention for assessment of integrin expression on (**B**) cMo, (**C**) iMo, and (**D**) ncMo via FACS. Data are represented as mean receptor number ± SD (two-way ANOVA with Tukey posttest, $*p < 0.05$ between healthy age-matched subject cohorts).

Monocyte arrest and transmigration on human aortic endothelial cells

Whole blood was layered over Lymphoprep (STEMCELL Technologies) and centrifuged at 1760 × g for 30 min followed by monocyte enrichment using STEMCELL Monocyte Enrichment Kit without CD16 depletion to 90% purity. Monocytes were concentrated to 10^6 cells/ml and labeled with CD14 AF488, CD16 AF647, and CCR2-PE Abs. Human aortic endothelial cells (HAECs) were grown to 90% confluency and treated for 4 h using 0.3 ng/ml TNF-α to promote upregulation of VCAM-1. Microfluidic chambers were reversibly adhered onto inflamed HAEC and monocytes perfused over the monolayer for 10 min at 2 dynes/cm^2 and imaged at 1-s intervals using a Nikon Eclipse TE2000-S microscope coupled to an Andor Zyla cMOS camera. Transmigration time and efficiency were determined using phase-contrast microscopy and fluorescent microscopy for the determination of monocyte subset arrest number and number of transmigrated cells.

Real-time phenotyping of monocytes in the A-Chip

Whole blood (50 μl) was treated with Human True Stain FcX and True Stain Monocyte Blocker prior to incubation with CD14 AF488 (HCD14), CD16 AF647 (3G8), and CCR2 PE (K036C2) Abs. Whole blood was diluted 1:3 with RPMI 1640 plus 5% FBS plus 0.1% HSA plus 1× penicillin/streptomycin and perfused into each microfluidic chamber at 2 dynes/cm^2. Fifteen distinct fields of view at 60× magnification were analyzed for each blood sample to quantify in total ∼150 monocytes per microfluidic channel (four channels per blood sample). Monocyte subset abundance was quantified by calibrating fluorescent signals derived from the CD14, CD16, and CCR2 primary Ab conjugates to receptor expression calculated using Bangs Laboratories beads with a known number of binding sites/area. Fresh Ab was added at 1:200 dilution for the duration of the experiment. For TIRF experiments, CD11c and CD49d expression were probed with mAbs BU15 and 9F10, respectively, and background was subtracted using fluorescently conjugated IgG controls. Images were taken every 5 min post–monocyte adhesion in the A-Chip for 60 min at a shear stress of 2 dynes/cm^2. For intracellular IL-1β measurements, whole blood was incubated with brefeldin A at a concentration of 5 μg/ml for 30 min at 37°C prior to perfusion into microfluidic chambers. Adherent monocytes were then fixed with 4% paraformaldehyde, permeabilized with BioLegend Intracellular Staining Permeabilization Wash Buffer (catalog no. 421002), and incubated with anti–IL-1β (clone JK1B-1) at a 1:100 concentration from the stock solution. Fluorescence was quantified using a Nikon Eclipse TE2000-S microscope coupled to an Andor Zyla cMOS camera using a 60× Apo TIRF oil objective (numerical aperture = 1.49). IL-1β measures were taken after 75 min. To account for nonspecific binding of anti–IL-1β, an IgG1k control conjugated to AF647 was used.

Receptor colocalization in lipid rafts

Isolated mononuclear cells were resuspended at 1 million/ml in 2 ml of chilled Dulbecco PBS without Ca^{2+} and Mg^{2+} following lipid raft labeling with Vybrant AF488 (Life Technologies) as per manufacturer's instructions. Lipid raft formation was inhibited using 10 mM methyl-β-cyclodextrin (Sigma Aldrich) for 30 min at 37°C. Cells were fixed with 1× fixation buffer (BioLegend) after 15 min of flow at 2 dynes/cm^2. Coverslips were mounted in Prolong Diamond Antifade Reagent (Life Technologies) for TIRF imaging using a Nikon Apo TIRF 60× oil objective (numerical aperture = 1.49). For colocalization analysis, monocytes were identified using DAPI nuclear stain to visualize the kidney

bean–shaped morphology specific to monocytes. ImageJ v1.51h was to identify the overlap between CD16 (red), CD11c (magenta), and lipid rafts (green).

Coimmunoprecipitation and Western blot

Human monocytes were isolated from whole blood by layering over a Lymphoprep density gradient, following enrichment via negative isolation. Isolated monocytes suspended in HBSS containing Ca^{2+} or Mg^{2+} and 0.1% HSA were perfused over glass coverslips functionalized with 10 μg/ml affinity modulating Abs 496B, 496K, or a pan-CD11c Ab (Bu15) at 2 dynes/cm^2 for 15 min, and captured cells were lysed (Pierce IP Lysis/Wash Buffer). Separately, protein G–coated magnetic beads from Dynabeads Protein G Immunoprecipitation Kit (Thermo Fisher Scientific) were incubated with 10 μg anti-CD11c (S-HCL-3) for 30 min. Lysates spin down for 30 min at 14,000 × *g* at 4°C, and supernatants were then incubated with the magnetic beads to pull down CD11c and associated molecules, which were magnetically separated and washed three times per manufacturer's recommendations. Samples were subjected to gel electrophoresis, and protein was transferred to a nitrocellulose membrane. The membrane was subsequently blocked with 5% milk for 2 h, and primary Ab was used to probe for CD11c (NBP-234491; R&D Systems), ADAM17 (ab57484; Abcam), CD16 (MEM-154; Sigma Aldrich), Syk (MA1-19332; Thermo Fisher Scientific), and p-Syk (44-233G; Thermo Fisher Scientific). An HRP-conjugated secondary Ab was used to stain primary Abs, and membranes were developed using ECL (SuperSignal West Femto Chemiluminescent Substrate; Pierce Biotechnology). Data from the blots were collected with ChemiDoc MP System, and the protein density was calculated using ImageJ and normalized to the intensity of the CD11c band.

ADAM17 inhibition

Isolated monocytes were resuspended at 1 million/ml in sterile filtered RPMI 1640 containing 0.1% human serum albumin and 10% FBS followed by labeling with Abs to CD14, CD16, and CCR2 and treatment with DMSO or 12 nM TMI-1, a selective ADAM17 inhibitor, for 30 min. Monocytes were perfused over a substrate of VCAM-1 for 75 min at 2 dynes/cm^2 in the presence of Ab and vehicle or ADAM17 inhibitor. Fluorescent measurements were taken at 5-min intervals, and receptor number was calculated with Quantum Simply Cellular beads to determine receptor number/time using a Nikon Eclipse TE2000-S microscope.

For NF-κB and IL-1β analysis, monocytes were pretreated with 5 μg/ml brefeldin A and 12 nM TMI-1 for 30 min at 37°C and perfused over a substrate of VCAM-1 for 2 h. Postshear, cells were fixed and permeabilized following incubation with 1:100 of anti–NF-κB p65 (clone: 1B12D11) PE and anti–IL-1β (clone: JK1B-1) AF647.

Cartoons were created using BioRender.

Statistics

Data are presented as mean ± SD, unless otherwise specified. Multiple groups were compared using one-way ANOVA with a Tukey posttest. All analysis was carried out using GraphPad Prism v7.02 for Windows (GraphPad Software, La Jolla, CA).

iMo integrin and chemokine receptor measures taken from CAD, NSTEMI, and healthy age-matched patients (n = 6) per group were transformed into an expression matrix and imported into RStudio (v3.4.1), where the data were normalized for multivariate analysis. Principal component analysis (PCA) provided an unbiased approach to separating healthy subjects by the integrin expression data. The hierarchical clustering of patient and healthy subjects as a function of each parameter is visualized in the heatmap depicting the coefficient of correlation. For the coimmunoprecipitation data in Supplemental Fig. 4 and the NF-κB and IL-1β expression data in Fig. 6, CAD and NSTEMI data points were combined following analysis by Student t test, which revealed no significant difference between these experimental groups.

Results

Integrin expression and chemokine receptors are upregulated to a greater extent on monocytes from cardiac patients than healthy patients

The efficiency of monocyte recruitment reflects the proportion that have adopted a primed state in the circulation, which is characterized by increased integrin activation and shear-resistant adhesion on endothelium at arterial sites of inflammation. Fresh whole blood samples were collected from CAD and NSTEMI patients on the day of percutaneous cardiac catheterization to examine monocyte heterogeneity in the expression and ex vivo function of adhesion and chemokine receptors as compared with venous blood from healthy age-matched subjects with no history of cardiovascular disease (Table I). Identification of monocyte subsets in whole blood by flow cytometry was based upon forward and side scatter parameters as well as the relative expression of CD14, CD16, HLA-DR, and CCR2 (Fig. 1A) (23). The relative frequency of each monocyte subset, classical monocyte (cMo) ($CD14^+$ $CD16^-$ $CCR2^+$; ∼80%), iMo ($CD14^+CD16^+CCR2^+$;∼10%), and nonclassical

Table I. Patient characteristics

	Healthy (n = 15)	CAD (n = 56)	NSTEMI (n = 46)
Male/female	10/5	32/24	32/14
Age (mean ± SD)	60 ± 6.62	60.76 ± 10.58	62.63 ± 10.32
BMI, kg/m^2 (mean ± SD)	25.1 ± 1.631	34.28 ± 8.862	27.93 ± 4.158
Diabetes (%)	0	24.14	34.78*
Hypertension (%)	41.6	88	82.6
Current smoker (%)	0	8.82	18.51*
LVEF%	None known	55.57 ± 9.55	48.125 ± 14.79
Culprit lesion	N/A	LM (3.57%), LAD (39.29%), Circ/OM (21.42%), RCA (32.14%), MVD (3.57%)	LM (11.4%), LAD (67.85%), Circ/OM (37.15)
Revascularization strategy	N/A	PCI/Med	PCI
Time to catheterization (min)	N/A	360.38 ± 818.30	861.38 ± 467.37
Hospital duration (h)	N/A	20.46 ± 14.74	61.44 ± 56.28
Medications preprocedure			
Antiplatelet (%)	N/A	75	78.2
Statins (%)	N/A	76.7	78.2
ACEI (%)	N/A	60.1	82.85
Beta blockers (%)	N/A	70.5	80
Medications postprocedure			
Antiplatelet (%)	N/A	77.27	87.8
Statins (%)	N/A	50	87.8
ACEI (%)	N/A	62.5	78.5
Beta blockers (%)	N/A	12.5	78.5

ACEI, angiotensin-converting enzyme inhibitor; BMI, body mass index; Circ/OM, circumflex arteries/obtuse marginal branches; LM, left main coronary artery; Med, medical therapy; MVD, microvasculature disease; PCI, percutaneous cardiac intervention; N/A, not applicable; RCA, right coronary artery.

Data represent the mean ± SD for the labeled categories or percentage of patients with a given condition or treatment.

*$p < 0.05$ comparing CAD and NSTEMI patients.

monocyte (ncMo) ($CD14^{dim}CD16^{+}CCR2^{-}$;~10%), was equivalent between cardiac patients and healthy subjects, although a larger variance was observed in the distributions of CAD and NSTEMI patients (Supplemental Fig. 1A–C). To gauge the activation state of circulating monocytes, integrin receptor expression of CD11c, CD11b, and VLA-4 was analyzed in whole blood samples fixed within 1 h of bedside collection (Fig. 1, Supplemental Fig. 1D–F). Membrane CD11c registered a baseline of ~20,000 receptors/cell in healthy age-matched subjects and was elevated ~2-fold on all monocyte subsets from patient samples (Fig. 1B–D). NSTEMI-derived iMo and ncMo exhibited the greatest increase in CD11c expression at ~2 fold above that of healthy samples. Coinciding with elevated CD11c expression on patients' iMo, a majority of CD11c receptors were shifted to a high affinity state with the greatest expression detected on NSTEMI compared with CAD, both of which exceeded the expression on monocytes from healthy age-matched subjects (Supplemental Fig. 1G). Chemokine receptors including CCR2, CCR5, and CX_3CR1 on monocytes endow them with the capacity to respond to inflammatory agonists, which motivated assessment of their expression on iMo (Supplemental Fig. 1H–J) (24, 25). Significantly higher CCR2 expression was detected on iMo from CAD, whereas CX_3CR1 expression on CAD and NSTEMI samples were double that detected on healthy subjects, indicative of a greater potential for inflammatory recruitment (Supplemental Fig. 1H–J). Notably, there was no detectable difference in monocyte frequency and equivalent trends in integrin expression from venous compared with arterial blood samples assayed in a subset of CAD patients, demonstrating the validity of comparing arterial samples from cardiac patients to venous samples collected from healthy age-matched subjects (data not shown).

Monocyte recruitment to inflamed endothelium is dependent on β_1- and β_2-integrin–mediated adhesion

To gauge the ex vivo proclivity of monocytes to activate and recruit to inflamed aortic endothelial cells, a confluent monolayer of arterial endothelium was stimulated with TNF-α to upregulate the integrin counterreceptors ICAM-1 and VCAM-1 along with inflammatory chemokines (26). Purified monocytes from patients and healthy subjects were labeled with fluorescent Abs to CD14, CD16, and CCR2 followed by perfusion through microfluidic channels at a physiological shear stress of 2 dynes/cm^2, and monocyte arrest and TEM were enumerated in real time (Fig. 2A). An equivalent number of cMo and iMo captured and transitioned to shear-resistant arrest, and an overall increase in the number of arrested cells from these subsets provided discrimination of the elevated recruitment efficiency of CAD and NSTEMI compared with healthy control samples (Fig. 2B, Supplemental Fig. 2A). Arrest efficiency was estimated to be ~10-fold higher for iMo (~1.5 per 100 perfused cells) compared with that of cMo and ncMo, given the ~10-fold lower frequency of iMo in whole blood. Moreover, nearly every arrested iMo proceeded to TEM at twice the rate of cMo, of which only ~30–40% were observed to undergo TEM (Supplemental Fig. 2A–C). In contrast, far fewer ncMo achieved arrest, and those that did were highly migratory yet inefficient at TEM, consistent with their reported propensity to patrol the vascular lumen (Supplemental Fig. 2B, 2E) (27).

Inhibition of integrin function by the addition of Abs that block ligand binding revealed a near complete dependence of monocyte arrest on VLA-4, regardless of monocyte subset or patient group (Fig. 2B, Supplemental Fig. 2). Moreover, cMo arrest and TEM was partially dependent on CD11c and CD11b (Supplemental Fig. 2A).

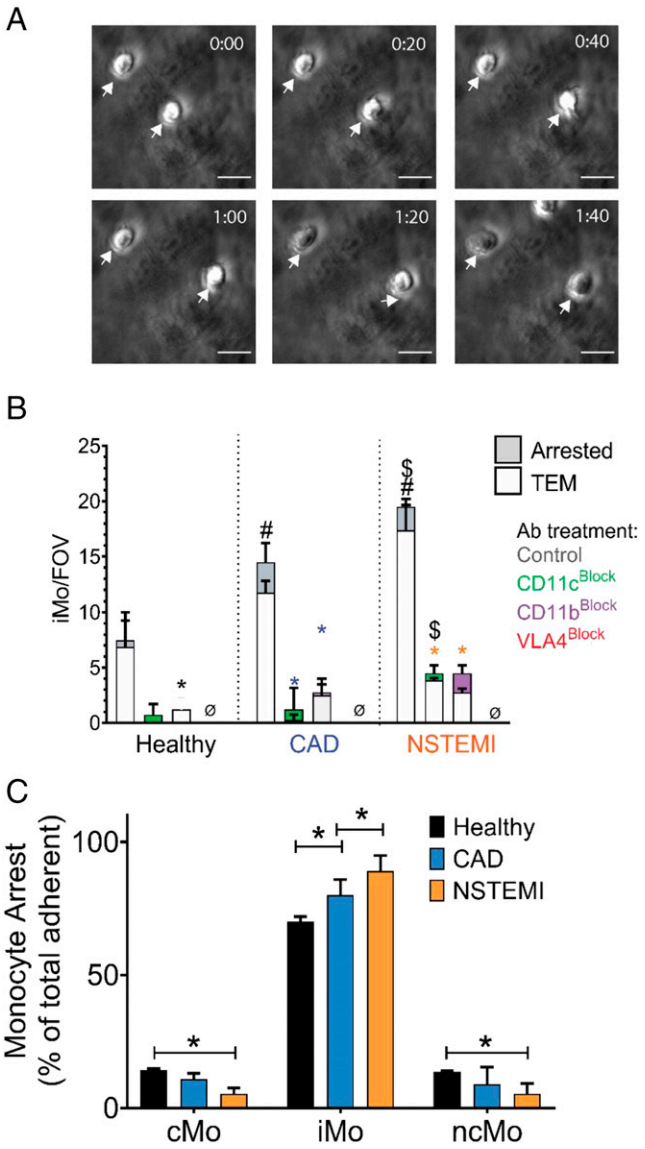

FIGURE 2. Monocyte recruitment to inflamed endothelium under shear stress is β_1- and β_2-integrin–dependent on binding to VCAM-1. (**A**) Monocytes were perfused into the A-Chip onto TNF-α–stimulated HAEC in the presence of blocking Abs to CD11c, CD11b, VLA-4, or a nonspecific isotype IgG (Control) and TEM of adherent cells (white arrows) assessed by phase-contrast imaging after 10 min of shear at 2 dynes/cm^2. Images display a time course of monocyte arrest and transmigration (phase dark) over 2 min. Scale bar, 10 μm. Monocyte subsets were determined based upon on-chip analysis of relative fluorescence intensity of Abs to CD14, CD16, and CCR2, which enabled the assessment of the number of arrested per field of view (FOV) at original magnification ×40. (**B**) Quantification of arrested iMo (filled bars) and the number of those arrested cells that have transmigrated (open bars) over 10 min of constant shear (2 dynes/cm^2). Data are represented as mean arrested or transmigrated cells per FOV ± SD (n = 4–5 per group) (two-way ANOVA with Tukey posttest $^{*}p < 0.05$ between isotype control within each cohort TEM color, $^{\#}p < 0.05$ compared with healthy, $^{\$}p < 0.05$ between CAD and NSTEMI cohorts for each Ab blocking treatment).(**C**) Monocyte subset arrest frequency on rVCAM-1 on the A-Chip. Data are represented as mean ± SD monocyte subset fraction of total arrested measured on the day of percutaneous coronary intervention or venous blood draw from healthy (n = 6), CAD (n = 8), and NSTEMI (n = 20) analyzed via two-way ANOVA with Tukey posttest. $^{*}p < 0.05$ between healthy age-matched subject groups.

iMo arrest displayed dependence on CD11c, CD11b, and VLA-4 for healthy and patient samples (Fig. 2B). NSTEMI samples exhibited the highest efficiency of transition from arrest to TEM that was more dependent upon VLA-4 activity as blocking CD11b and CD11c were less effective, as reported (28–30). These data confirm previous findings indicating that monocyte arrest is dependent upon activation of β_2-integrins, whereas TEM is dependent predominately upon VLA-4 function (6, 28, 30, 31).

Monocyte recruitment from whole blood on VCAM-1 requires signaling between high affinity CD11c and VLA-4 to activate shear-resistant stable adhesion (15). To directly quantify the efficiency of monocyte arrest for CAD and NSTEMI patients compared with healthy controls, whole blood samples were perfused at a defined shear stress on a substrate of rVCAM-1 within microfluidic channels in the A-Chip. iMo arrest efficiency was computed from the total number that achieved stable adhesion normalized by each patient's monocyte count in blood. Consistent with the capture of isolated monocytes on inflamed aortic endothelium, arrest efficiency of iMo from whole blood was ~7–10 fold higher than that of cMo and ncMo assayed from the same individuals (Fig. 2C). Moreover, the arrested fraction of iMo increased, with disease severity reaching ~80% in CAD and ~90% of total adherent monocytes per field of view from blood of NSTEMI patients compared with ~70% in healthy samples (Fig. 2C). It is noteworthy that arrest efficiency was equivalent whether blood was collected from arterial or venous blood vessels as assessed in samples collected from a subset of CAD patients (data not shown).

We next sought to confirm if higher arrest efficiency measured for patient versus healthy iMo was dependent upon the capacity for high affinity CD11c to activate VLA-4 binding to VCAM-1 (Fig. 3A), as previously reported (2, 15). Pretreatment of isolated monocytes with an allosteric Ab that binds the I-domain of CD11c and stabilizes a low affinity conformation ($CD11c^{LA}$) resulted in a ~50% reduction in iMo arrest across all healthy subjects compared with a control anti-$CD11c^{IgG}$ that recognizes a common epitope. Furthermore, complete abrogation of iMo arrest in the presence of a function blocking anti–VLA-4 Ab was observed, consistent with its role in arrest on inflamed endothelium.

To assess how the increase in arrest efficiency of iMo correlates with integrin and chemokine receptor expression, we performed a regression analysis between CD11c, CD11b, VLA-4, and CX3CR1 and the number of iMo recruited in the A-Chip from patient versus healthy controls (Fig. 3B–E). Of the integrin receptors, only CD11c yielded a significant positive linear correlation with iMo arrest frequency for each healthy subject group (healthy: slope = 2.0, $r = 0.74$, $p = 0.01$; CAD: slope = 1.2, $r = 0.87$, $p = 0.004$; and NSTEMI: slope = 1.0, $r = 0.86$, $p = 0.0001$). A similar correlation was observed between VLA-4 expression and iMo arrest for healthy and NSTEMI patients (healthy: slope = 0.60, $r = 0.76$, $p = 0.06$; CAD: slope = 0.40, $r = 0.67$, $p = 0.99$; and NSTEMI: slope = 0.41, $r = 0.76$, $p = 0.04$). However, the relative increase in iMo arrest on VCAM-1 per rise in VLA-4 receptor expression was less in comparison to the steep slope and tight correlation between arrest and CD11c receptor expression that provided discrimination of NSTEMI from CAD and healthy controls.

To further gauge whether the integrin and chemokine receptor expressed on iMo could discriminate between patients and healthy subjects, we conducted a multivariate analysis of the expression data. An unsupervised hierarchical K-means PCA analysis of six individuals randomly chosen from each subject group identified three expression clusters from the cohort, which precisely coincided with the separation of healthy, CAD, and NSTEMI samples into discrete groupings (Fig. 3F). Of the parameters, CX3CR1 and CCR2 expression on iMo depicted in the heatmap provided the strongest discrimination of patients identified post-analysis as CAD, whereas common epitope and high affinity CD11c receptor expression were the most faithful parameters in grouping NSTEMI patients (Fig. 3G).

CD16 expression on arrested iMo is differentially regulated by a shift in CD11c affinity and ADAM17 proteolytic activity

The arrest and migration of monocytes on inflamed endothelium involves the diffusion of high affinity CD11c into focal adhesion complexes enriched in membrane raft domains in which p-Syk and paxillin convert VLA-4 to a high affinity state that supports shear-resistant arrest on VCAM-1 (15). To examine the dynamics in diffusion of CD11c and VLA-4 receptors, monocytes in blood samples from healthy and cardiac patients were labeled with distinct fluorescence reporters and imaged by TIRF microscopy within the optical plane of membrane adhesion (i.e., ~100 nM) on arrested iMo. Fluorescence intensity of CD11c within sites of focal adhesion registered a continuous increase from an equivalent baseline number of bound receptors detected following arrest ($t = 0$) under shear flow. Notably, the baseline expression of VLA-4 receptors on iMo at the time point of arrest was 3-fold higher in patients (CAD: 663.5 $\pm$ 180.2 mean fluorescence intensity [MFI]; NSTEMI: 632.5 $\pm$ 130.0 MFI) than that of healthy samples (113.2 $\pm$ 19.61 MFI) (Supplemental Fig. 3A, 3B). Integrin density within focal clusters rose to a maximum within 15–25 min in samples from healthy subjects and cardiac patients (Fig. 4A–C). Typically, CD11c receptor accumulation, from a similar baseline level in healthy and cardiac iMo (Supplemental Fig. 3A), led the rise in VLA-4 bond formation, resulting in coalescence in high density integrin clusters at sites of focal contact. Remarkable is the observation that CD11c and VLA-4 bond density diminished over time subsequent to the rise and returned to the baseline expression value for iMo from CAD and NSTEMI patients but not healthy controls in which integrin levels remained elevated (Fig. 4C).

To further examine how the observed dynamics of CD11c and VLA-4 expression correlated with subsequent shifts in iMo phenotype in healthy compared with patient samples, we next assessed alterations in membrane expression of CD14, CD16, and CCR2 following arrest on VCAM-1. Monocyte membrane-associated CD14 and CCR2 did not exhibit significant changes in expression over time (data not shown). However, the vast majority of arrested iMo derived from healthy subjects (~95%) exhibited a continuous increase in CD16 expression over 25 min, reaching a peak at ~3-fold (CD16: 26,700 $\pm$ 15,700 receptors/cell) above the baseline of ~10,000 receptors/cells (Fig. 4D, 4E). Coinciding with this increase was the coalescence of CD16 and CD11c within micron-sized clusters enriched in membrane lipid rafts at sites of focal adhesion (Supplemental Fig. 3C–F), a process that required continuous exposure to fluid shear stress (Fig. 4E). In contrast, the majority of adherent iMo derived from CAD and NSTEMI patients underwent a continuous decrease in CD16 expression (Fig. 4D, 4E). Significant loss from the baseline of ~10,000 CD16 receptors was detected after 30 min for CAD iMo (CD16: 5600 $\pm$ 8400 receptors/cell) and 15 min for NSTEMI iMo (CD16: 2560 $\pm$ 5520 receptors/cell) (Fig. 4D, 4E). Notable is the observation that loss of CD16 was coincident with the decrease in CD11c and VLA-4 expression within focal adhesions (Fig. 4). This process, henceforth denoted "phenotypic conversion," characterized by the shedding of CD16 to undetectable levels, occurred in ~60% of patient-derived iMo. By comparison, a much smaller fraction of

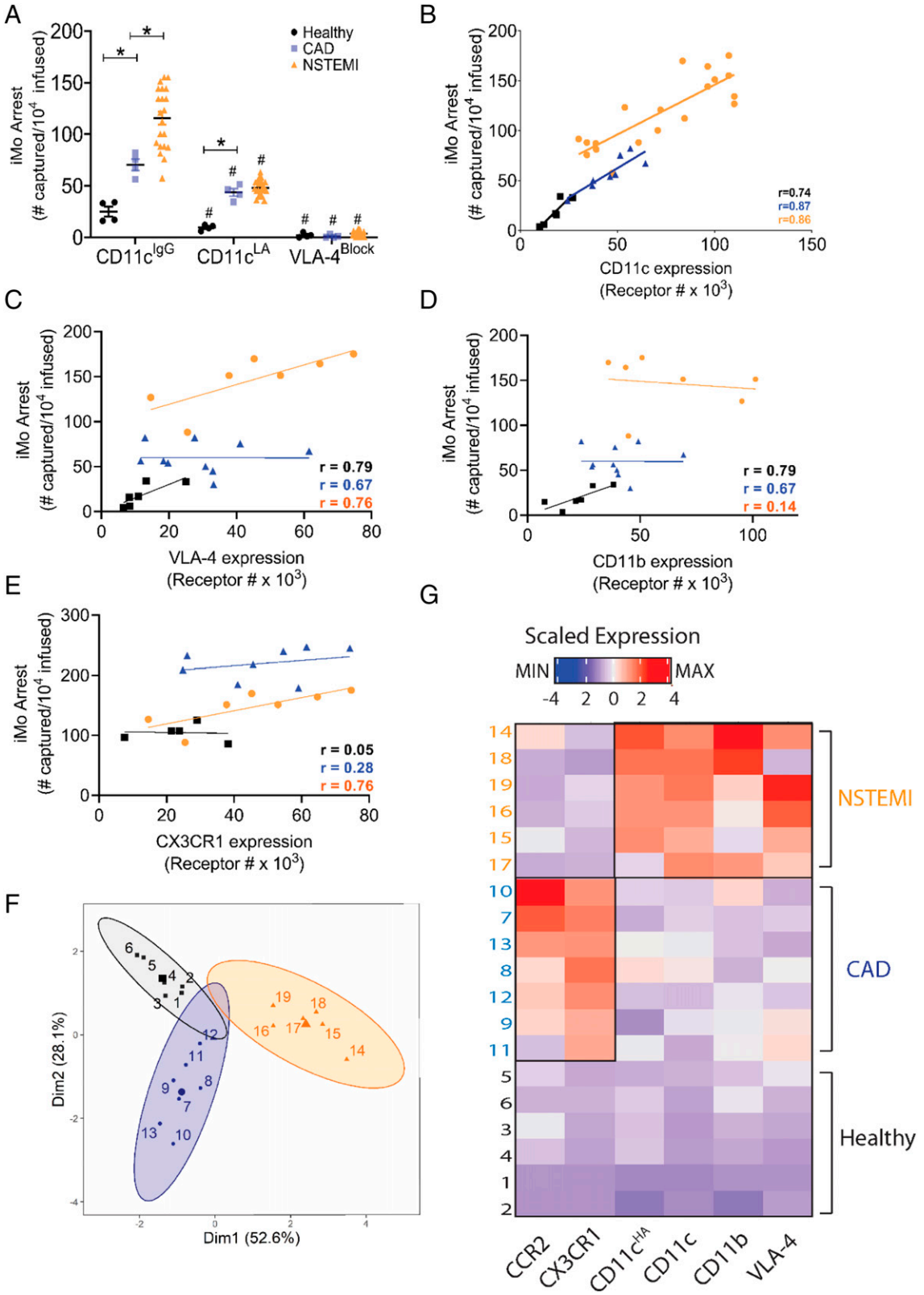

FIGURE 3. Recruitment of iMo on VCAM-1 is regulated by the expression level and affinity state of CD11c, which discriminates cardiac patients from healthy controls. (**A**) Integrin dependence of iMo arrest following treatment with a pan–anti-CD11c mAb to a nonblocking common epitope (IgG), an allosteric anti-CD11c low affinity–inducing mAb, and anti–VLA-4 functional blocking mAb (healthy, $n = 5$; CAD, $n = 5$; NSTEMI, $n = 21$). Data are represented as mean ± SD iMo arrest number (two-way ANOVA with Tukey posttest, $^{*}p < 0.05$ between patient groups, $^{\#}p < 0.05$ from the anti-CD11c IgG control). Arrest fraction of iMo/10,000 monocytes infused into the A-Chip plotted against an individual patient's mean receptor number for (**B**) CD11c ($n = 6$, healthy; $n = 8$, CAD; $n = 20$, NSTEMI), (**C**) VLA-4 ($n = 6$, healthy; $n = 10$, CAD; $n = 7$, NSTEMI), (**D**) CD11b ($n = 6$, healthy; $n = 10$, CAD; $n = 7$, NSTEMI), and (**E**) CX3CR1 ($n = 6$, healthy; $n = 8$, CAD; $n = 7$, NSTEMI) receptor expression measured on whole blood monocytes via FACS analysis with the resulting Pearson correlation. (**F**) Principle component plot of integrin and chemokine receptor expression from six random individuals from each of the healthy, CAD, and NSTEMI groups, in which each data point represents a unique individual. The plot represents a *(Figure legend continues)*

iMo (~5%) from healthy subjects exhibited CD16 shedding, and in all samples, phenotypic conversion required the presence of shear stress (Fig. 4E). It was also noted that although ncMo arrested within the A-Chip registered similar CD16 expression compared with iMo, they did not alter expression over the 60 min of observation under shear stress, regardless of the subject group from which they were derived (data not shown).

It is reported that upon activation of neutrophils and NK cells, outside-in signaling through CD11b engaged to ICAM-1 elicits CD16 clustering and shedding, which in turn leads to enhanced cell motility (32–35). This motivated scrutiny of the relationship between CD11c affinity and changes in CD16 expression following arrest on VCAM-1. Allosteric Abs that stabilize a high or low affinity state were compared with a control anti-CD11c IgG that recognizes a common epitope. Each Ab was separately infused into the A-Chip immediately following monocyte arrest under shear flow while continuously monitoring receptor expression and membrane redistribution of CD11c and CD16. Stabilizing CD11c in a high affinity conformation ($CD11c^{HA}$) elicited a significant increase in colocalization with CD16 within lipid raft domains enriched at sites of focal adhesions (Fig. 4D, Supplemental Fig. 3). Notably, disruption of lipid rafts via methyl-β-cyclodextrin prevented the colocalization of CD11c and CD16, indicative of the formation of a signaling complex (Supplemental Fig. 3). Induction of $CD11c^{HA}$ abrogated conversion of iMo defined by the absence of CD16 shedding, which remained at the baseline static level for nearly all subjects, save a small fraction (~10%) of NSTEMI samples (Fig. 4F). In contrast, stabilizing CD11c in a low affinity ($CD11c^{LA}$) conformation following monocyte arrest induced shedding of CD16 and phenotypic conversion within 15–25 min of Ab addition into the flow channel and at the highest rate in NSTEMI samples. Taken together, phenotypic conversion of iMo is initiated within minutes of shear-resistant arrest on VCAM-1 and is triggered by a shift in CD11c conformation from high to low affinity that is marked by coalescence of VLA-4 and shedding of CD16.

Cleavage of CD16 on innate immune cells is regulated through ADAM17, a metalloproteinase known to act on NK cells and neutrophils undergoing β_2-integrin–mediated migration (36–38). To determine if ADAM17 enrichment on circulating iMo accounts for the difference in propensity for CD16 shedding and increase in phenotypic conversion observed in patients compared with heathy controls, we measured surface expression by flow cytometry on monocytes in whole blood samples. ADAM17 receptors were expressed at equivalent levels and frequency (~50–75%) across all monocyte subsets with no significant difference detected between healthy subjects and patients (Supplemental Fig. 4A, 4B).

We next examined the physical association of CD11c, CD16, and ADAM17 within sites of focal contact by capturing monocytes on VCAM-1 in the A-Chip under static or flow conditions and performing TIRF immunofluorescence on intact cells and Western blot on cell lysates collected from microfluidic channels (Fig. 5A–I, Supplemental Fig. 4C–F). Fig. 5A depicts the putative colocalization of the three receptors within the plane of adhesion at focal contacts just after iMo arrest on the VCAM-1 as confirmed by the representative TIRF images (Fig. 5B). A Pearson correlation analysis of the imaging data revealed a close association between CD11c bonds with CD16 and ADAM17 in focal clusters that occurred to an equivalent extent in healthy, CAD, and NSTEMI patients (Fig. 5C, 5D).

To assess outside-in signaling as a function of CD11c affinity regulation under shear and static conditions, we probed for the phosphorylation of Syk within focal adhesion complexes as depicted in the illustration of Fig. 5E. In the presence and absence of shear stress and allosteric stabilizing Abs, arrested monocytes from healthy, CAD, and NSTEMI patients were lysed and immunoprecipitated using anti-CD11c as the capture Ab (Fig. 5F–I, Supplemental Fig. 4). Densitometry applied to the Western blots reveal that under static conditions, regardless of affinity state, CD11c precipitated equivalent levels of Syk, CD16, and ADAM17. Stabilizing CD11c at high affinity in the presence of shear stress significantly increased the amount of CD16 pulled down, and this corresponded to a 4-fold increase in p-Syk within the complex compared with iMo stabilized at low affinity by the addition of anti-CD11c or under static conditions. The capacity for $CD11c^{HA}$ to cocluster with CD16 and induce p-Syk in the presence of ADAM17 was equivalent between CAD, NSTEMI, and healthy samples (Supplemental Fig. 4C–F).

To evaluate whether the proteolytic activity of ADAM17 is necessary to induce the shedding of CD16 and trigger phenotypic conversion of iMo as observed in CAD and NSTEMI and depicted in Fig. 5J, patient samples were treated with the ADAM17 selective inhibitor TMI-1 compared with a vehicle control. Inhibition of ADAM17 effectively attenuated CD16 shedding on patient's iMo, which maintained a baseline level of $\sim 10^4$ receptors over 75 min (Fig. 5K, 5L). By comparison, samples receiving vehicle control shed CD16 with typical kinetics of iMo undergoing conversion. Taken together, these data reveal that iMo all express proteolytically competent ADAM17, and following arrest on VCAM-1, CD16 diffuses into sites of focal adhesion within lipid rafts and coalesce with high affinity CD11c and VLA-4 bonds in a process that requires fluid shear stress and is associated with outside-in signaling as indicated by p-Syk activation. A subsequent shift in CD11c from high to low affinity coincides with ADAM17-mediated cleavage of CD16, which marks the phenotypic conversion of a majority of iMo from CAD and NSTEMI patients and, to a far lesser extent, those from healthy age-matched subjects.

Conversion of iMo to a proinflammatory state is dynamically regulated by a shift in the affinity state of CD11c

Nuclear translocation of NF-κB is a critical step in acute activation of monocytes, resulting in the secretion of proinflammatory mediators involved in CAD morbidity and associated with plaque erosion during MI (39). To investigate whether shedding of CD16 on iMo corresponds to the execution of an acute inflammatory transcriptional program, we imaged arrested iMo for nuclear translocation of NF-κB and elaboration of IL-1β following 2 h of culture under continuous shear stress. To examine the role of CD11c affinity, we quantified NF-κB and IL-1β expression in the presence of allosteric stabilizing anti-CD11c Abs (Fig. 6A, 6B). Following shear-resistant arrest on VCAM-1 in the A-Chip, a small fraction of iMo (~5%) from healthy patients shed CD16, which coincided with nuclear translocation of ~50% of cytosolic NF-κB corresponding to the baseline measurement. In contrast, a majority of iMo (~75%) from CAD and NSTEMI patients

two-dimensional space that contains 80.7% of the original expression data, in which the *x*-axis or dimension 1 (Dim1) represents 52.6% of the original expression data, and the *y*-axis given by dimension 2 (Dim2) represents 28.1% of the original input of expression data. (**G**) Heatmap of the integrin and chemokine receptor parameters used in the principal component clustering analysis. Relative weighting of the correlations depicted by a gradient in which blue is the minimum, white (0) is the median, and red indicates the maximum.

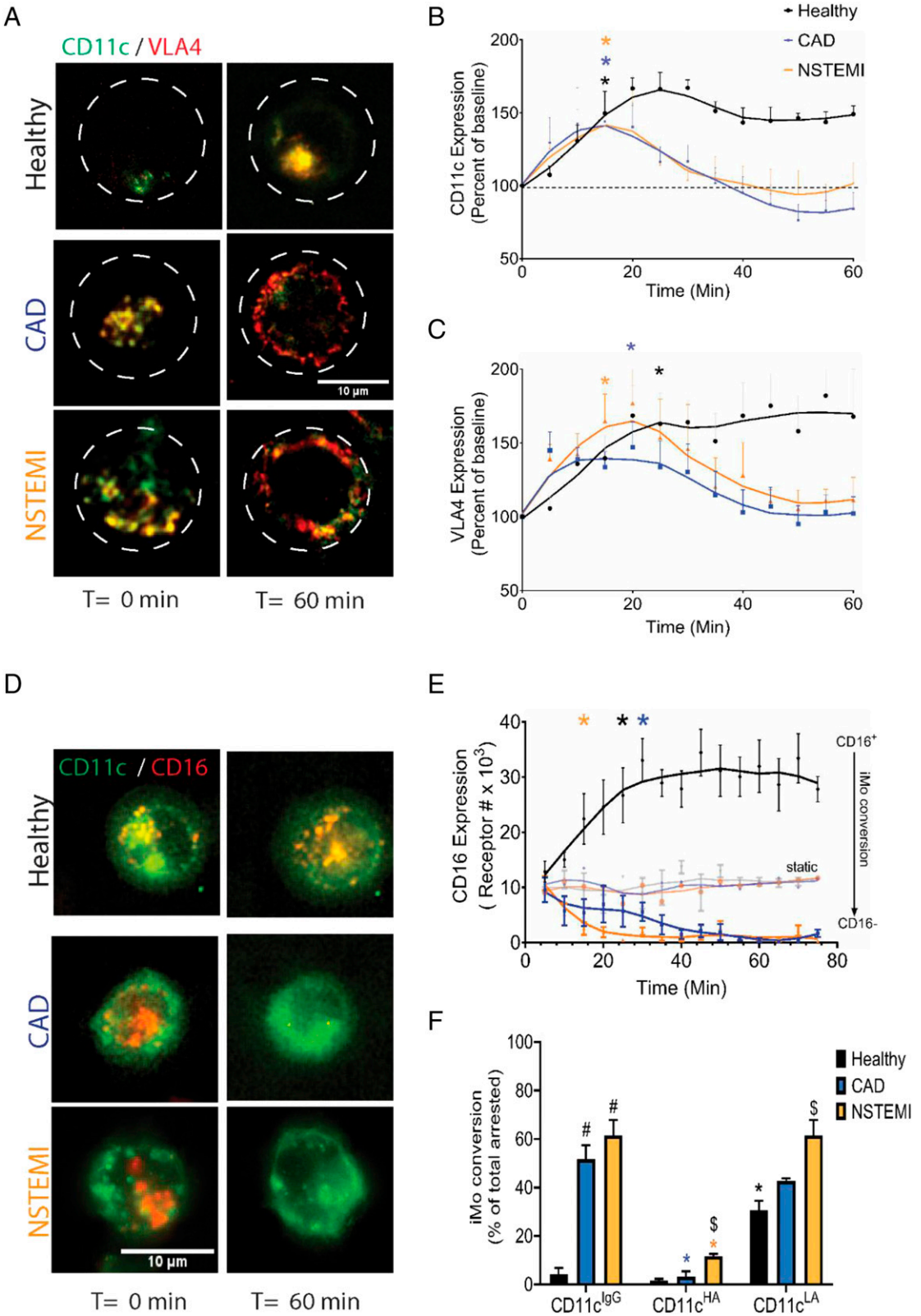

FIGURE 4. iMo form focal adhesions through activated CD11c and diffusion of VLA-4 that precedes conversion to a CD16$^-$ phenotype postarrest on VCAM-1. (**A**) TIRF images of iMo CD11c (green) and VLA-4 (red) expression at time of attachment to human rVCAM-1 ($T = 0$) and at 60 min postarrest at 2 dynes/cm^2 shear stress for healthy, CAD, and NSTEMI (scale bar, 10 µm). Quantification of healthy (black, $n = 7$), CAD (blue, $n = 7$), and NSTEMI (orange, $n = 5$) iMo (**B**) CD11c and (**C**) CD49d (VLA-4) membrane receptor MFI per cell area at time of arrest to establish baseline fluorescence/cell area (bar graphs) and dynamically over time using live TIRF. Data are represented as percentage change from baseline fluorescence at the time of attachment for CD11c or VLA-4 receptors (one-way ANOVA with Tukey posttest, $^*p < 0.05$ comparing the maximal percentage change to the baseline at $T = 0$. Scale bar, 10 µm). (**D**) Representative images of iMo from healthy, CAD, and NSTEMI patients depict CD16 expression (red) and CD14 (green) at $t = 0$ min (time of arrest) and 60 min postarrest. (**E**) CD16 receptor expression on adherent iMo assessed from the time of capture to 60 min postadhesion from healthy ($n = 6$), CAD ($n = 7$), and NSTEMI ($n = 5$) patients under constant flow or under static conditions (translucent points and lines). *(Figure legend continues)*

increased NF-κB nuclear translocation up to 150% of the healthy baseline signal. Stabilization of high affinity CD11c effectively blocked nuclear translocation of NF-κB in CAD and NSTEMI samples down to the baseline level (Fig. 6A). In contrast, stabilization of low affinity CD11c maintained the level of NF-κB in iMo from CAD and NSTEMI equivalent to treatment with the control anti-CD11c^{IgG} Ab. To assess if activation of NF-κB induced the expression of proinflammatory cytokines, we assayed for cytosolic IL-1β, which is associated with enhanced incidence of CAD and the onset of MI (40). Isolated monocytes were treated with brefeldin A to limit extracellular secretion of protein generated over 2 h of shear-resistant cell arrest. Consistent with the observed extent of NF-κB nuclear translocation, IL-1β expression was inhibited by stabilizing CD11c in a high affinity conformation (Fig. 6B). In contrast, stabilizing low affinity CD11c initiated a significant increase in IL-1β production that was expressed at the highest level in phenotypically converted iMo from NSTEMI, whereas lower levels were detected in CAD compared with the baseline in healthy samples (Fig. 6B). It is noteworthy that iMo from healthy patients were resistant to allosteric induction of NF-κB and IL-1β in the presence of anti-CD11c^{LA}. We conclude that a spontaneous downshift in CD11c affinity within adhesive sites consolidated by VLA-4/VCAM-1 bond formation on arrested iMo hastens proinflammatory polarization of converted iMo from cardiac patients but not healthy age-matched subjects.

To further assess the regulatory function of ADAM17 metalloprotease in conversion to an inflammatory phenotype, we measured nuclear translocation of NF-κB and IL-1β production on arrested iMo under shear stress in the presence or absence of the proteolytic inhibitor TMI-1 (Fig. 6C, 6D). Compared with the ~150% increase in NF-κB and IL-1β observed in monocytes treated with anti-CD11c^{IgG} or anti-CD11c^{LA} allosteric inducer in the CAD and NSTEMI samples, TMI-1 effectively blocked NF-κB translocation and IL-1β production down to the baseline detected in healthy controls. Moreover, the presence of the ADAM17 inhibitor prevented the decrease in expression of CD11c and CD16 within sites of focal contact observed in iMo from cardiac samples (Supplemental Fig. 4G–I). We conclude that conversion of CAD- and NSTEMI-derived iMo to an inflammatory phenotype is regulated by a spontaneous shift in CD11c from high to low affinity under bond tension that is marked by shedding of CD16 and regulated by ADAM17 proteolytic function.

Upregulation of CD11c and enhanced iMo recruitment in the A-Chip correlate with the extent of myocardial injury assessed at the onset of MI

To assess whether inflammatory activation of iMo is related to the extent of myocardial injury and infarction, we correlated clinical measures of coronary injury in NSTEMI patients with the level of integrin expression on iMo and the efficiency of arrest on VCAM-1 in the A-Chip. Of the integrins regressed, only the rise in CD11c expression on iMo revealed a significant positive correlation with increased levels of serum creatine kinase (CK-MB) and peak troponin measured in NSTEMI patients (Fig. 7A, 7B). An inverse correlation was revealed by plotting mean CD11c receptor level versus the left ventricular ejection fraction (LVEF%) for each NSTEMI patient. This plot depicts a progressive decrease in cardiac contractility with elevation in CD11c expression on patients' iMo (Fig. 7C). Importantly, we found that the capture efficiency of iMo in the A-Chip was elevated by an additional 50% consistently in a small subset of patients experiencing a recurrent event within 3 y of their primary NSTEMI (Fig. 7D). These correlations underscore the importance of CD11c expression and function in governing iMo recruitment that plays a central role in the pathogenesis of CAD.

Discussion

Monocytes released into the blood from the bone marrow and spleen constitute a heterogenous population that varies in health and disease. This is evident in the relative capacity and fraction within each subset to recruit to inflamed arteries and adopt a proatherogenic phenotype. Through examination of monocyte inflammatory responses postrecruitment on VCAM-1 within the A-Chip, we gauged the magnitude and variance of inflammatory function among a cohort consisting of high risk albeit stable cardiovascular patients and those who experienced a primary or recurrent MI. Perfusion of patient blood through the A-Chip provided an ex vivo means of stratifying CAD and NSTEMI patients that led to the following findings: 1) iMo from NSTEMI patients registered the highest expression levels of integrin receptors that coincided with the greatest efficiency of arrest and diapedesis on inflamed aortic endothelium; 2) the capacity for CD11c to activate VLA-4 dependent arrest on VCAM-1 in the A-Chip increased in direct proportion to markers of myocardial injury and was consistently elevated in a subset of patients experiencing a repeat MI; 3) on-chip analysis of the fate of iMo arrested under shear revealed that a majority of those from cardiac patients and, rarely, healthy age-matched subjects converted to a proatherogenic phenotype; and 4) activation of an inflammatory transcriptional program was mechanoregulated through a focal adhesion complex consisting of CD11c, VLA-4, CD16, ADAM17, and p-Syk. We conclude that the presence of fluid shear stress acting on high affinity integrin bonds is necessary to mechanotransduce outside-in signaling that converts a subset of iMo toward an inflammatory phenotype. Phenotypic conversion consistent with an inflammatory state was greatest in NSTEMI patients and required metalloprotease activity of ADAM17 and subsequent cleavage of CD16 that coincided with activation of NF-κB and elaboration of IL-1β. Diagnosing and targeting the earliest events in arterial recruitment and inflammatory conversion of circulating monocytes could provide a strategy for preventing the progression of CAD patients to MI and prevent the high morbidity and mortality of atherosclerosis disease.

Priming and activation of monocytes in circulation

Circulating monocytes in hypercholesterolemic apoE$^{-/-}$ mice fed a high-fat Western diet upregulate CD36 scavenger receptor and the signaling protein low-density lipoprotein receptor-related protein 1 that mediates the uptake of cholesterol-rich lipoproteins. These monocytes, which are considered the murine homolog of iMo, become foamy within weeks of the onset of a high-fat diet and upregulate chemokine receptors CCR2, CX_3CR1, and CD11c

iMo conversion was classified as expressing fewer than 10,000 receptors, which was equivalent to background nonspecific fluorescence intensity. Data are represented as mean CD16 receptor number at time of arrest to VCAM-1 (one-way ANOVA with Tukey posttest, $*p < 0.05$ comparing the peak increase/decrease the baseline at $T = 0$. Scale bar, 10 μm). (**F**) Fraction of iMo that have converted relative to baseline CD16 receptor expression from healthy ($n = 6$), CAD ($n = 7$), and NSTEMI ($n = 7$) patients at 75 min under constant shear and treatment with CD11c allosteric or a pan-CD11c Ab control. Data are represented as mean CD16 expression/time ± SD (two-way ANOVA with Tukey posttest, $^{\#}p < 0.05$ compared with healthy controls, $*p < 0.05$ compared with the CD11c IgG treatment for each healthy age-matched subject cohort, $^{\$}p < 0.05$ between CAD and NSTEMI). Scale bar, 10 μm.

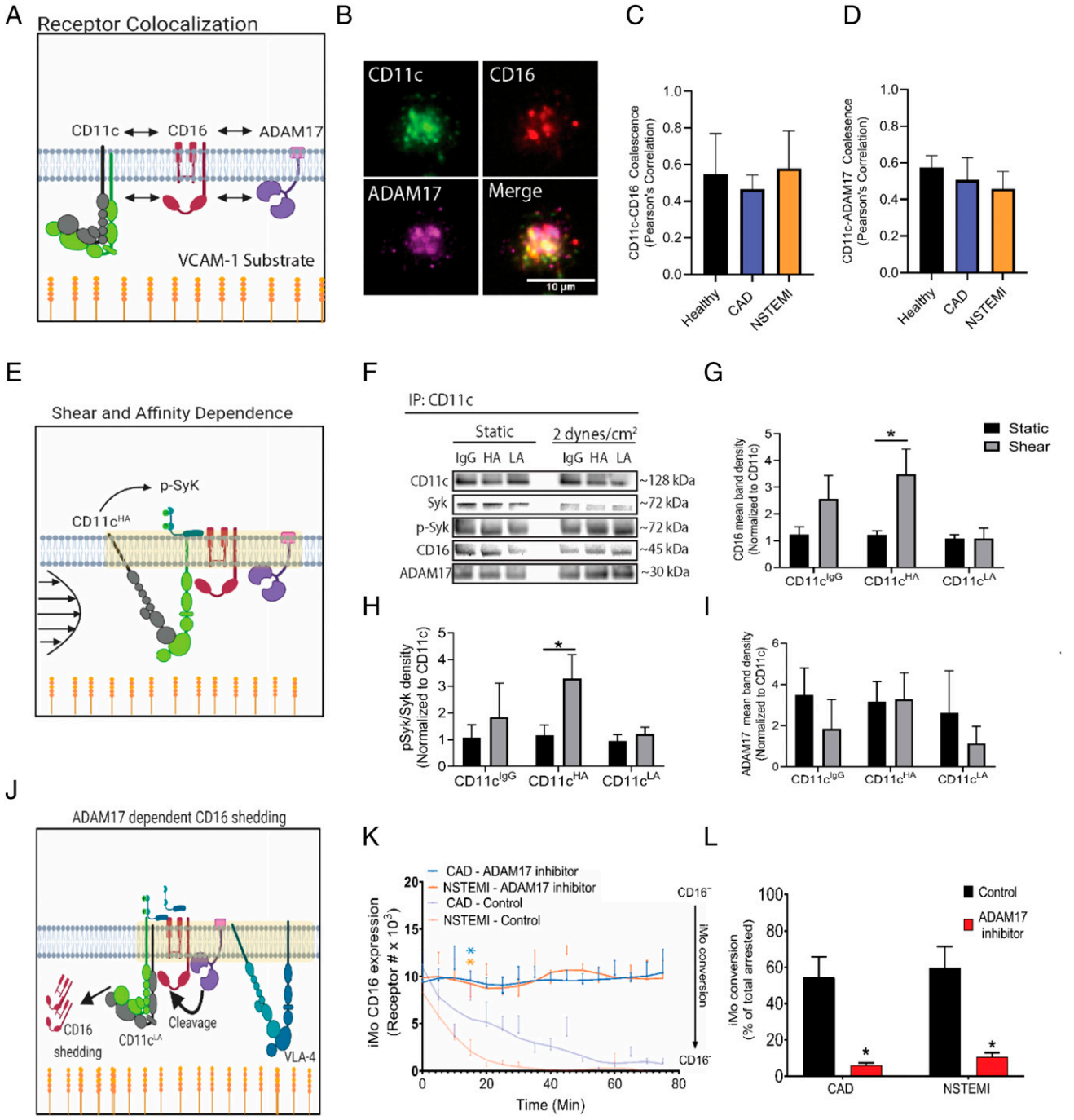

FIGURE 5. An allosteric shift in CD11c affinity following iMo arrest on VCAM-1 induces membrane coalescence with CD16 and subsequent cleavage by ADAM17. (**A**) Schematic depicting the coalescence and (**B**) immunofluorescent images of CD11c (green), ADAM17 (purple), and CD16 (red) within focal adhesive contact on VCAM-1 at the time point of capture (scale bar, 10 μm). Associated Pearson correlation of the coalescence of membrane (**C**) CD11c–CD16 and (**D**) CD11c–ADAM17 receptors under static conditions from healthy, CAD, and NSTEMI iMo (n = 4–5). (**E**) Schematic representation of high affinity CD11c coclustered with CD16. This results in outside-in signaling associated with phosphorylation of Syk and association with ADAM17. (**F**) Western blot of coimmunoprecipitation of CD11c with ADAM17 and CD16 and associated signaling component p-Syk following 15 min of shear stress or static conditions on arrested monocytes from a healthy donor using allosteric affinity modulating mAbs to CD11c or a pan anti-CD11c control IgG (n = 7). (**G**) CD16, (**H**) p-Syk/Total Syk, and (**I**) ADAM17 band density normalized to CD11c protein expression quantified by densitometry (n = 7). Data are represented as mean band intensity normalized to CD11c ± SD (Student t test, $^*p < 0.05$ between static and shear conditions) (n = 7). (**J**) Schematic representation of phenotypic conversion dependent upon ADAM17-mediated cleavage of CD16 and an allosteric shift to low affinity CD11c at focal sites of VLA-4–mediated adhesion. (**K**) ADAM17-dependent cleavage of CD16 on iMo from CAD and NSTEMI when treated with ADAM17 inhibitor (TMI-1 at 12 nM) (translucent lines) or DMSO vehicle control (filled lines) over 75 min at 2 dynes/cm^2 postarrest to VCAM-1. * represents a significant difference between vehicle and TMI-1 at the given time point that is sustained after 15 min of shear. One-way ANOVA with Tukey posttest, $^*p < 0.05$. (**L**) iMo conversion frequency after 75 min of shear postarrest to VCAM-1 in the presence of ADAM17 inhibitor or vehicle control. Data are represented as mean conversion ± SD (Student t test. $^*p < 0.05$ between treated and vehicle control).

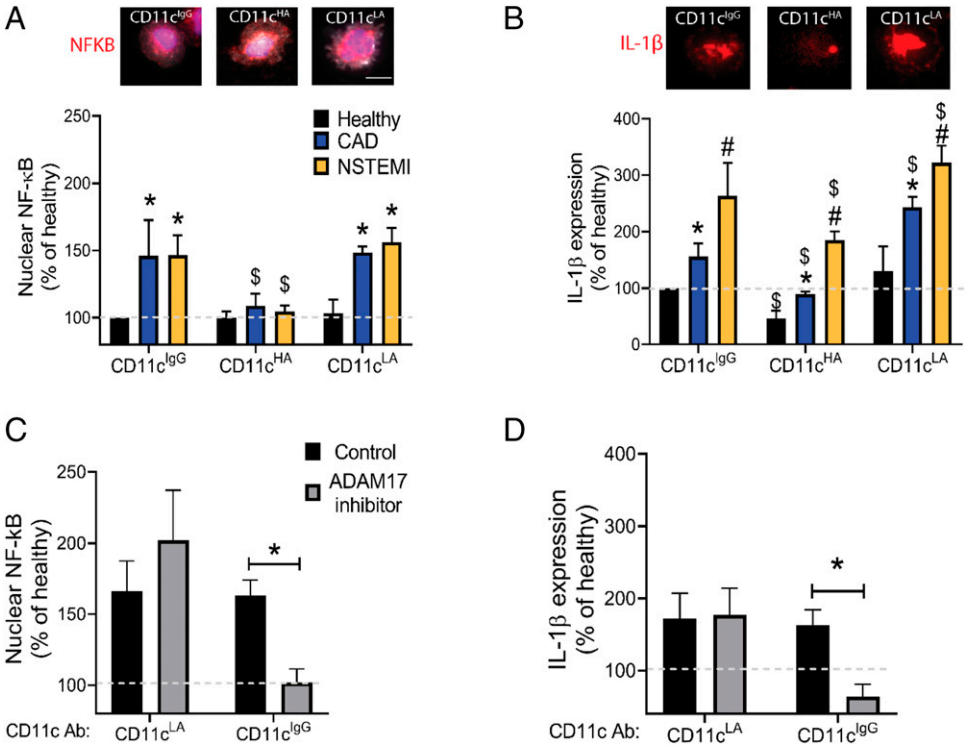

FIGURE 6. Conversion of iMo to an inflammatory phenotype is associated with nuclear translocation of NF-κB and production of IL-1β that requires ADAM17 proteolytic activity. (**A**) NF-κB cytosolic to nuclear translocation ($n = 6$/group). (**B**) Intracellular IL-1β production in brefeldin A–treated iMo at 2 h of shear and treatment with allosteric affinity stabilizing anti-CD11c or IgG control that binds the common epitope of CD11c ($n = 6$ per group) (two-way ANOVA with Tukey posttest, $^{*}p < 0.05$ from control within each Ab treatment, $^{\#}p < 0.05$ between CAD and NSTEMI within Ab treatments, $^{\$}p < 0.05$ from the CD11c IgG treatment for each patient cohort). (**C**) Combined expression of nuclear NF-κB ($n = 4$; CAD; $n = 2$, NSTEMI) and (**D**) cytosolic IL-1β ($n = 3$ CAD, $n = 2$ NSTEMI) after treatment with ADAM17 inhibitor TMI-1 or vehicle in the presence of the IgG control to CD11c or the low affinity promoting Ab after 2 h of shear-resistant arrest to VCAM-1 at 2 dynes/cm^2. Two-way ANOVA with Tukey posttest, $^{*}p < 0.05$ from the control treatment compared with that of the ADAM17 inhibitor.

(2, 9). Assessment of ex vivo monocyte recruitment from these mice revealed a 2-fold increase in arrest on VCAM-1 in the A-Chip commensurate with upregulated CD11c expression, a process that was absent in hypercholesterolemic CD11c$^{-/-}$ mice. Furthermore, CD11c^{+} foamy monocytes express activated VLA-4 necessary for shear-resistant cell arrest and infiltration into nascent lesions, which correlates with the high density of CD11c^{+} macrophages detected in inflamed arteries (9). Likewise, iMo in the circulation of CAD and NSTEMI patients registered significantly higher CD11c receptor expression and a greater propensity to recruit on VCAM-1 and convert to an inflammatory phenotype under shear stress.

iMo phenotypic conversion in the A-Chip points to an inflammatory role in atherosclerosis

There is ample evidence that significant shifts in monocyte phenotype and fate specification can have a profound impact on the atherosclerosis progression and patient outcome post-MI. In humans, alterations in the milieu of circulating monocytes that favor an increased frequency of iMo is commensurate with increased atherosclerotic burden and the risk of fatal heart attack and ischemic stroke (10, 14, 41). These observations led to the premise that iMo represents the cardinal CD11c^{+} CCR2^{+} monocyte in disease progression that is endowed with a high propensity to recruit and efficiently transmigrate to inflamed vessels at hemodynamically atherosusceptible regions of plaque formation (42). Consistent with iMo being the predominant inflammatory cell infiltrate, they have been observed in the arterial intima of post mortem cardiac tissue in patients who experienced acute MI (13, 42). In assessing blood monocyte activation states from cardiac patients with clinical symptoms ranging from angina to fatigue and blocked arteries, we found an enhanced capacity for iMo recruitment demonstrated by significant upregulation of high affinity membrane CD11c and VLA-4 in CAD and NSTEMI patients. The frequency of iMo arrest in the A-Chip provided an ex vivo metric to assess the capacity to arrest in inflamed arteries and polarize toward a proatherogenic phenotype in cardiac patients. Two functional readouts of monocyte activation effectively discriminated between healthy subjects and CAD or NSTEMI patients. Bivariate analysis of the relative extent of CD11c receptor upregulation versus monocyte recruitment efficiency for each patient provided a reliable parameter for discrimination between CAD and NSTEMI patients compared with healthy subjects. Applying a multivariate PCA based upon receptor expression of chemokine and integrin receptors on iMo revealed that integrin upregulation and CD11c activation provided the strongest discrimination between NSTEMI, CAD, and healthy subjects. We interpret that this unbiased statistical ranking in receptor expression that emerged in CAD and NSTEMI highlights an increased propensity for iMo recruitment and chemotaxis at arterial sites of nascent plaque formation. Supporting this is a report that CX3CR1^{+} monocytes that release CCL2 facilitate and positively regulate CCR2^{+} inflammatory monocyte recruitment and lesion growth in CAD (43). Although signaling through CCR2 can upregulate and activate CD11c, it is unknown if signaling through CX3CR1 also modulates its affinity and outside-in signaling that determines changes in the phenotype of iMo. Integrin expression metrics in NSTEMI patients also increased in direct proportion to their rise in serum in CK-MB, troponin T, and deceases in LVEF%

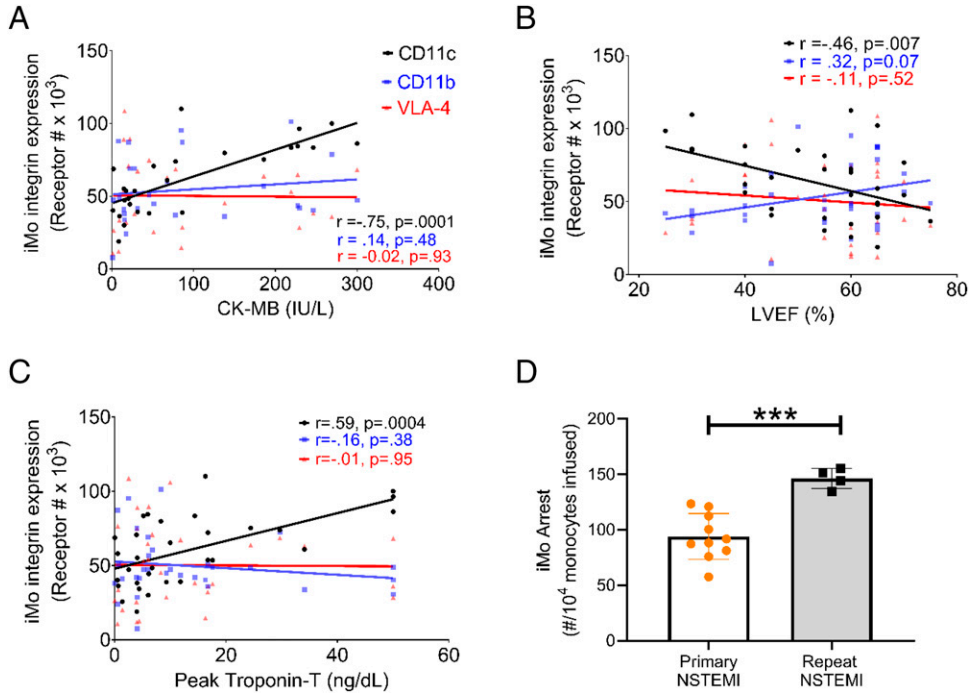

FIGURE 7. Integrin expression and iMo arrest as a function of measures of myocardial injury and incidence of MI in cardiac patients. Bivariate plots of iMo average integrin receptor expression (CD11c [black]; CD11b [blue]; VLA-4 [red]) from each NSTEMI patient versus corresponding serum measures of (**A**) CK-MB, (**B**) LVEF%, (**C**) and peak troponin T (CD11c: $n = 33$; CD11b: $n = 30$; VLA-4: $n = 31$), with resulting Pearson correlation coefficient. (**D**) Number of iMo arrested under shear stress in the A-Chip from patients experiencing a primary NSTEMI ($n = 9$) versus those returning to the clinic for a repeat MI within 3 y ($n = 4$). Student t test $^{***}p < 0.001$.

that provides a readout of the extent of myocardial injury and the potential for recurrence of MI, further highlighting a critical role of CD11c in disease progression. Abrogation of iMo arrest was achieved by pretreatment with Ab that stabilizes CD11c at low affinity or with function blocking anti–VLA-4. These data confirmed the cooperativity between high affinity CD11c and activation of VLA-4–dependent arrest. We report in this study that recruitment efficiency increased to the greatest extent in CAD patients who have progressed to MI. These findings are consistent with previous reports that iMo capture on the A-Chip under shear stress is sufficient to activate VLA-4 via outside-in signaling through CD11c and shear-dependent Syk phosphorylation (19, 44, 45). This highlights the important role played by β_1- and β_2-integrins in iMo recruitment and their capacity to alter iMo fate by signaling conversion to a proatherogenic state, which can participate in plaque erosion that exacerbates vascular pathology ranging from angina to MI.

Integrin allosteric regulation of monocyte phenotypic conversion observed ex vivo in the A-Chip

Integrin-mediated immune modulation of arrested monocytes can provide crucial stimuli that can promote or inhibit inflammatory activation of these cells once resident in tissues. Of these, β_2-integrins have been reported to promote anti-inflammatory phenotypes in monocyte-derived dendritic cells, whereas β_1-integrins such as VLA-4 promote proinflammatory activation in tissue macrophages through NF-κB (46, 47). As evidence for this, recruitment of iMo from blood samples of CAD and NSTEMI proceeded to adopt a proinflammatory phenotype in the presence of shear stress that was triggered by the conformational downshift in CD11c affinity that initiated VLA-4–mediated outside-in signaling. Within focal sites of adhesive contact on VCAM-1, integrin activation and deactivation through a downshift in CD11c affinity following its diffusion from focal adhesions initiated ADAM17-dependent cleavage of the ectodomain of CD16, which preceded NF-κB translocation and production of IL-1β. Stabilizing high affinity CD11c, or preventing the shedding of CD16 with the ADAM17 antagonist, effectively blocked nuclear translocation of NF-κB and diminished production of IL-1β in the A-Chip. Phenotypic conversion required the presence of fluid shear stress, which implicates a tensile force acting on high affinity CD11c in transducing signals, leading to a coalescence of CD16, p-Syk, and VLA-4 in a complex stabilized within membrane lipid rafts. A similar mechanism has been reported in adipose-associated macrophages, in which phosphorylation of Syk via the Fcγ-chain induces VLA-4 activation (46). However, these data are the first, to our knowledge, to demonstrate that a downshift in CD11c affinity postrecruitment is required for activation of the proteolytic activity of ADAM17 and resultant CD16 shedding, which marked phenotypic conversion of a majority of iMo in CAD and NSTEMI patients. ADAM17 expression and the extent of CD16 shedding was highest on iMo from NSTEMI and far less prevalent on monocytes from healthy age-matched subjects, whose cells upon arrest retained high affinity CD11c and exhibited a time-dependent upregulation in CD16 membrane expression. A healthy patient's iMo exhibited a low baseline level of NF-κB translocation and maintained a stable noninflammatory phenotype in the presence of shear stress in the A-Chip. Allosteric stabilization of low affinity CD11c on healthy and patients' iMo was sufficient to activate ADAM17 and trigger inflammatory conversion. These data are consistent with reports that ADAM17 activity coincides with macrophage accumulation, atherosclerosis burden, and the activity of MMPs in plaque destabilization in patients presenting with acute MI (48). Noteworthy is the observation that although stabilization of high affinity CD11c prevented ADAM17-mediated cleavage of CD16 and the subsequent nuclear translocation of NF-κB, it did not prevent CD11c-dependent outside-in activation of p-Syk and its induction of high affinity VLA-4/VCAM-1 bonds. Activation of VLA-4 via Fcγ-chain induction of PI3kγ activity on inflammatory

monocytes leads to a PI3K/Akt signaling pathway and activation of AP-1 response genes that stabilize inflammatory transcription factors such as HIF-1α (47, 49). These data reveal a mechanism by which outside-in signaling through CD11c and its colocalization and regulation of CD16 through ADAM17 effectively promotes VLA-4 activation that is required for the subsequent NF-κB translocation and initiation of an AP-1–associated proinflammatory program. Further, these data implicate ADAM17 on monocytes as a proteolytic regulator of inflammatory function downstream of CD11c mechanotransduction.

Clinical relevance

The mortality rate in patients experiencing recurrent MI within 3 y of the primary incident is ∼9% and approaches 50% at 10 y. This underscores a critical need to stratify patients based upon the intensity of their inflammatory disease and treat those at greatest risk for mortality with intensive cardiac rehabilitation. The recent Canakinumab Anti-Inflammatory Thrombosis Outcome Study clinical trial highlighted the seminal role of IL-1β–dependent inflammation in propagating incidence of MI; however, morbidity and mortality was not reduced (50). This highlights the utility of limiting inflammation in patients but underscores the multifaceted nature of the disease.

iMo represent a key player in the progression of atherosclerosis; however, accurate measures of their functional capacity to polarize and secrete inflammatory cytokines in relation to disease are limited. In this regard, applying the A-Chip to assess the ex vivo inflammatory response of circulating monocytes can provide a baseline readout of a patient's inflammatory status but also their likelihood to respond favorably to therapeutic intervention.

Acknowledgments

We appreciate the generous provision of allosteric Abs to CD11c by Dr. Robert Benschop of Eli Lilly Corp.

Disclosures

The authors have no financial conflicts of interest.

References

1. Bäck, M., A. Yurdagul, Jr., I. Tabas, K. Öörni, and P. T. Kovanen. 2019. Inflammation and its resolution in atherosclerosis: mediators and therapeutic opportunities. *Nat. Rev. Cardiol.* 16: 389–406.
2. Foster, G. A., R. M. Gower, K. L. Stanhope, P. J. Havel, S. I. Simon, and E. J. Armstrong. 2013. On-chip phenotypic analysis of inflammatory monocytes in atherogenesis and myocardial infarction. *Proc. Natl. Acad. Sci. USA* 110: 13944–13949.
3. Gower, R. M., H. Wu, G. A. Foster, S. Devaraj, I. Jialal, C. M. Ballantyne, A. A. Knowlton, and S. I. Simon. 2011. CD11c/CD18 expression is upregulated on blood monocytes during hypertriglyceridemia and enhances adhesion to vascular cell adhesion molecule-1. *Arterioscler. Thromb. Vasc. Biol.* 31: 160–166.
4. Cybulsky, M. I., and M. A. Gimbrone, Jr 1991. Endothelial expression of a mononuclear leukocyte adhesion molecule during atherogenesis. *Science* 251: 788–791.
5. Cybulsky, M. I., K. Iiyama, H. Li, S. Zhu, M. Chen, M. Iiyama, V. Davis, J. C. Gutierrez-Ramos, P. W. Connelly, and D. S. Milstone. 2001. A major role for VCAM-1, but not ICAM-1, in early atherosclerosis. *J. Clin. Invest.* 107: 1255–1262.
6. Sadhu, C., H. J. Ting, B. Lipsky, K. Hensley, L. F. Garcia-Martinez, S. I. Simon, and D. E. Staunton. 2007. CD11c/CD18: novel ligands and a role in delayed-type hypersensitivity. *J. Leukoc. Biol.* 81: 1395–1403.
7. Konstantopoulos, K., S. Kukreti, and L. V. McIntire. 1998. Biomechanics of cell interactions in shear fields. *Adv. Drug Deliv. Rev.* 33: 141–164.
8. Wu, H., R. M. Gower, H. Wang, X. Y. Perrard, R. Ma, D. C. Bullard, A. R. Burns, A. Paul, C. W. Smith, S. I. Simon, and C. M. Ballantyne. 2009. Functional role of CD11c+ monocytes in atherogenesis associated with hypercholesterolemia. *Circulation* 119: 2708–2717.
9. Xu, L., X. Dai Perrard, J. L. Perrard, D. Yang, X. Xiao, B. B. Teng, S. I. Simon, C. M. Ballantyne, and H. Wu. 2015. Foamy monocytes form early and contribute to nascent atherosclerosis in mice with hypercholesterolemia. *Arterioscler. Thromb. Vasc. Biol.* 35: 1787–1797.
10. Rogacev, K. S., B. Cremers, A. M. Zawada, S. Seiler, N. Binder, P. Ege, G. Große-Dunker, I. Heisel, F. Hornof, J. Jeken, et al. 2012. CD14++CD16+ monocytes independently predict cardiovascular events: a cohort study of 951 patients referred for elective coronary angiography. *J. Am. Coll. Cardiol.* 60: 1512–1520.
11. Imanishi, T., H. Ikejima, H. Tsujioka, A. Kuroi, K. Ishibashi, K. Komukai, T. Tanimoto, Y. Ino, T. Takeshita, and T. Akasaka. 2010. Association of monocyte subset counts with coronary fibrous cap thickness in patients with unstable angina pectoris. *Atherosclerosis* 212: 628–635.
12. Kashiwagi, M., T. Imanishi, H. Tsujioka, H. Ikejima, A. Kuroi, Y. Ozaki, K. Ishibashi, K. Komukai, T. Tanimoto, Y. Ino, et al. 2010. Association of monocyte subsets with vulnerability characteristics of coronary plaques as assessed by 64-slice multidetector computed tomography in patients with stable angina pectoris. *Atherosclerosis* 212: 171–176.
13. Tsujioka, H., T. Imanishi, H. Ikejima, A. Kuroi, S. Takarada, T. Tanimoto, H. Kitabata, K. Okochi, Y. Arita, K. Ishibashi, et al. 2009. Impact of heterogeneity of human peripheral blood monocyte subsets on myocardial salvage in patients with primary acute myocardial infarction. *J. Am. Coll. Cardiol.* 54: 130–138.
14. Dong, S., W. Ji, S. Zeng, J. Miao, L. Yan, X. Liu, J. Liu, X. Zhou, and Q. Yang. 2020. Admission low-density lipoprotein cholesterol stratified by circulating CD14++CD16+ monocytes and risk for recurrent cardiovascular events following ST elevation myocardial infarction: lipid paradox revised. *J. Cardiovasc. Transl. Res.* DOI: 10.1007/s12265-020-10015-6.
15. Foster, G. A., L. Xu, A. A. Chidambaram, S. R. Soderberg, E. J. Armstrong, H. Wu, and S. I. Simon. 2015. CD11c/CD18 signals very late antigen-4 activation to initiate foamy monocyte recruitment during the onset of hypercholesterolemia. *J. Immunol* 195: 5380–5392.
16. Lin, T. H., A. Yurochko, L. Kornberg, J. Morris, J. J. Walker, S. Haskill, and R. L. Juliano. 1994. The role of protein tyrosine phosphorylation in integrin-mediated gene induction in monocytes. *J. Cell Biol.* 126: 1585–1593.
17. Reyes-Reyes, M., N. Mora, G. Gonzalez, and C. Rosales. 2002. beta1 and beta2 integrins activate different signalling pathways in monocytes. *Biochem. J.* 363: 273–280.
18. Dong, X., Z. Zheng, P. Lin, X. Fu, F. Li, J. Jiang, and P. Zhu. 2020. ACPAs promote IL-1β production in rheumatoid arthritis by activating the NLRP3 inflammasome. *Cell. Mol. Immunol.* 17: 261–271.
19. McGilvray, I. D., Z. Lu, R. Bitar, A. P. Dackiw, C. J. Davreux, and O. D. Rotstein. 1997. VLA-4 integrin cross-linking on human monocytic THP-1 cells induces tissue factor expression by a mechanism involving mitogen-activated protein kinase. *J. Biol. Chem.* 272: 10287–10294.
20. Shaw, R. J., D. E. Doherty, A. G. Ritter, S. H. Benedict, and R. A. Clark. 1990. Adherence-dependent increase in human monocyte PDGF(B) mRNA is associated with increases in c-fos, c-jun, and EGR2 mRNA. *J. Cell Biol.* 111: 2139–2148.
21. Bajpai, G., C. Schneider, N. Wong, A. Bredemeyer, M. Hulsmans, M. Nahrendorf, S. Epelman, D. Kreisel, Y. Liu, A. Itoh, et al. 2018. The human heart contains distinct macrophage subsets with divergent origins and functions. *Nat. Med.* 24: 1234–1245.
22. Dick, S. A., J. A. Macklin, S. Nejat, A. Momen, X. Clemente-Casares, M. G. Althagafi, J. Chen, C. Kantores, S. Hosseinzadeh, L. Aronoff, et al. 2019. Self-renewing resident cardiac macrophages limit adverse remodeling following myocardial infarction. [Published erratum appears in 2019 *Nat. Immunol*. 20: 664.] *Nat. Immunol.* 20: 29–39.
23. Thomas, G. D., A. A. J. Hamers, C. Nakao, P. Marcovecchio, A. M. Taylor, C. McSkimming, A. T. Nguyen, C. A. McNamara, and C. C. Hedrick. 2017. Human blood monocyte subsets: a new gating strategy defined using cell surface markers identified by Mass cytometry. *Arterioscler. Thromb. Vasc. Biol.* 37: 1548–1558.
24. Patel, A. A., Y. Zhang, J. N. Fullerton, L. Boelen, A. Rongvaux, A. A. Maini, V. Bigley, R. A. Flavell, D. W. Gilroy, B. Asquith, et al. 2017. The fate and lifespan of human monocyte subsets in steady state and systemic inflammation. *J. Exp. Med.* 214: 1913–1923.
25. Yona, S., K. W. Kim, Y. Wolf, A. Mildner, D. Varol, M. Breker, D. Strauss-Ayali, S. Viukov, M. Guilliams, A. Misharin, et al. 2013. Fate mapping reveals origins and dynamics of monocytes and tissue macrophages under homeostasis. [Published erratum appears in 2013 *Immunity* 38: 1073–1079.] *Immunity* 38: 79–91.
26. Sun, C., K. Alkhoury, Y. I. Wang, G. A. Foster, C. E. Radecke, K. Tam, C. M. Edwards, M. T. Facciotti, E. J. Armstrong, A. A. Knowlton, et al. 2012. IRF-1 and miRNA126 modulate VCAM-1 expression in response to a high-fat meal. *Circ. Res.* 111: 1054–1064.
27. Thomas, G., R. Tacke, C. C. Hedrick, and R. N. Hanna. 2015. Nonclassical patrolling monocyte function in the vasculature. *Arterioscler. Thromb. Vasc. Biol.* 35: 1306–1316.
28. Weber, C., and T. A. Springer. 1998. Interaction of very late antigen-4 with VCAM-1 supports transendothelial chemotaxis of monocytes by facilitating lateral migration. *J. Immunol.* 161: 6825–6834.
29. Chuluyan, H. E., and A. C. Issekutz. 1993. VLA-4 integrin can mediate CD11/CD18-independent transendothelial migration of human monocytes. *J. Clin. Invest.* 92: 2768–2777.
30. Shang, X. Z., B. J. Lang, and A. C. Issekutz. 1998. Adhesion molecule mechanisms mediating monocyte migration through synovial fibroblast and endothelium barriers: role for CD11/CD18, very late antigen-4 (CD49d/CD29), very late antigen-5 (CD49e/CD29), and vascular cell adhesion molecule-1 (CD106). *J. Immunol.* 160: 467–474.
31. Ting, H. J., J. P. Stice, U. Y. Schaff, D. Y. Hui, J. C. Rutledge, A. A. Knowlton, A. G. Passerini, and S. I. Simon. 2007. Triglyceride-rich lipoproteins prime aortic endothelium for an enhanced inflammatory response to tumor necrosis factor-alpha. *Circ. Res.* 100: 381–390.
32. Goodier, M. R., C. Lusa, S. Sherratt, A. Rodriguez-Galan, R. Behrens, and E. M. Riley. 2016. Sustained immune complex-mediated reduction in CD16 expression after vaccination regulates NK cell function. *Front. Immunol.* 7: 384.

33. Middelhoven, P. J., J. D. van Buul, M. Kleijer, D. Roos, and P. L. Hordijk. 1999. Actin polymerization induces shedding of FcgammaRIIIb (CD16) from human neutrophils. *Biochem. Biophys. Res. Commun.* 255: 568–574.
34. Srpan, K., A. Ambrose, A. Karampatzakis, M. Saeed, A. N. R. Cartwright, K. Guldevall, G. D. S. C. De Matos, B. Önfelt, and D. M. Davis. 2018. Shedding of CD16 disassembles the NK cell immune synapse and boosts serial engagement of target cells. *J. Cell Biol.* 217: 3267–3283.
35. Stöckl, J., O. Majdic, W. F. Pickl, A. Rosenkranz, E. Prager, E. Gschwantler, and W. Knapp. 1995. Granulocyte activation via a binding site near the C-terminal region of complement receptor type 3 alpha-chain (CD11b) potentially involved in intramembrane complex formation with glycosylphosphatidylinositol-anchored Fc gamma RIIIB (CD16) molecules. *J. Immunol.* 154: 5452–5463.
36. Romee, R., B. Foley, T. Lenvik, Y. Wang, B. Zhang, D. Ankarlo, X. Luo, S. Cooley, M. Verneris, B. Walcheck, and J. Miller. 2013. NK cell CD16 surface expression and function is regulated by a disintegrin and metalloprotease-17 (ADAM17). *Blood* 121: 3599–3608.
37. Jing, Y., Z. Ni, J. Wu, L. Higgins, T. W. Markowski, D. S. Kaufman, and B. Walcheck. 2015. Identification of an ADAM17 cleavage region in human CD16 (FcγRIII) and the engineering of a non-cleavable version of the receptor in NK cells. *PLoS One* 10: e0121788.
38. Tsubota, Y., J. M. Frey, P. W. L. Tai, R. E. Welikson, and E. W. Raines. 2013. Monocyte ADAM17 promotes diapedesis during transendothelial migration: identification of steps and substrates targeted by metalloproteinases. *J. Immunol.* 190: 4236–4244.
39. Kawano, S., T. Kubota, Y. Monden, T. Tsutsumi, T. Inoue, N. Kawamura, H. Tsutsui, and K. Sunagawa. 2006. Blockade of NF-kappaB improves cardiac function and survival after myocardial infarction. *Am. J. Physiol. Heart Circ. Physiol.* 291: H1337–H1344.
40. Morton, A. C., A. M. Rothman, J. P. Greenwood, J. Gunn, A. Chase, B. Clarke, A. S. Hall, K. Fox, C. Foley, W. Banya, et al. 2015. The effect of interleukin-1 receptor antagonist therapy on markers of inflammation in non-ST elevation acute coronary syndromes: the MRC-ILA Heart Study. *Eur. Heart J.* 36: 377–384.
41. Grosse, G. M., W. J. Schulz-Schaeffer, O. E. Teebken, R. Schuppner, M. Dirks, H. Worthmann, R. Lichtinghagen, G. Maye, F. P. Limbourg, and K. Weissenborn. 2016. Monocyte subsets and related chemokines in carotid artery stenosis and ischemic stroke. *Int. J. Mol. Sci.* 17: 433.
42. Mangold, A., T. M. Hofbauer, A. S. Ondracek, T. Artner, T. Scherz, W. S. Speidl, K. A. Krychtiuk, R. Sadushi-Kolici, J. Jakowitsch, and I. M. Lang. 2019. Neutrophil extracellular traps and monocyte subsets at the culprit lesion site of myocardial infarction patients. *Sci. Rep.* 9: 16304.
43. Tacke, F., D. Alvarez, T. J. Kaplan, C. Jakubzick, R. Spanbroek, J. Llodra, A. Garin, J. Liu, M. Mack, N. van Rooijen, et al. 2007. Monocyte subsets differentially employ CCR2, CCR5, and CX3CR1 to accumulate within atherosclerotic plaques. *J. Clin. Invest.* 117: 185–194.
44. Campbell, I. D., and M. J. Humphries. 2011. Integrin structure, activation, and interactions. *Cold Spring Harb. Perspect. Biol.* 3: a004994.
45. Zohlnhöfer, D., K. Brand, K. Schipek, G. Pogatsa-Murray, A. Schömig, and F. J. Neumann. 2000. Adhesion of monocyte very late antigen-4 to endothelial vascular cell adhesion molecule-1 induces interleukin-1beta-dependent expression of interleukin-6 in endothelial cells. *Arterioscler. Thromb. Vasc. Biol.* 20: 353–359.
46. Chung, K. J., A. Chatzigeorgiou, M. Economopoulou, R. Garcia-Martin, V. I. Alexaki, I. Mitroulis, M. Nati, J. Gebler, T. Ziemssen, S. E. Goelz, et al. 2017. A self-sustained loop of inflammation-driven inhibition of beige adipogenesis in obesity. *Nat. Immunol.* 18: 654–664.
47. Podgrabinska, S., O. Kamalu, L. Mayer, M. Shimaoka, H. Snoeck, G. J. Randolph, and M. Skobe. 2009. Inflamed lymphatic endothelium suppresses dendritic cell maturation and function via Mac-1/ICAM-1-dependent mechanism. *J. Immunol.* 183: 1767–1779.
48. Zhao, X., J. Kong, Y. Zhao, X. Wang, P. Bu, C. Zhang, and Y. Zhang. 2015. Gene silencing of TACE enhances plaque stability and improves vascular remodeling in a rabbit model of atherosclerosis. *Sci. Rep.* 5: 17939.
49. Totsuka, N., Y. G. Kim, K. Kanemaru, K. Niizuma, E. Umemoto, K. Nagai, S. Tahara-Hanaoka, C. Nakahasi-Oda, S. Honda, M. Miyasaka, et al. 2014. Toll-like receptor 4 and MAIR-II/CLM-4/LMIR2 immunoreceptor regulate VLA-4-mediated inflammatory monocyte migration. *Nat. Commun.* 5: 4710.
50. Ridker, P. M., B. M. Everett, T. Thuren, J. G. MacFadyen, W. H. Chang, C. Ballantyne, F. Fonseca, J. Nicolau, W. Koenig, S. D. Anker, et al; CANTOS Trial Group. 2017. Antiinflammatory therapy with canakinumab for atherosclerotic disease. *N. Engl. J. Med.* 377: 1119–1131.